Huete, C., Sánchez, A. L., Williams, F. A. & Urzay, J. (2015). Diffusion-flame ignition by shock-wave impingement on a supersonic mixing layer. *Journal of Fluid Mechanics, 784*, pp. 74–108.

DOI: 10.1017/jfm.2015.585

Diffusion-flame ignition by shock-wave impingement on a supersonic mixing layer

César Huete[1], Antonio L. Sánchez[1] †, Forman A. Williams[1], and Javier Urzay[2]

[1]Department of Mechanical and Aerospace Engineering, University of California, San Diego, 9500 Gilman Dr., La Jolla, CA 92093-0411, USA

[2]Center for Turbulence Research, Stanford University, Stanford, CA 94305-3024, USA

(Received ?; revised ?; accepted ?. - To be entered by editorial office)

Ignition in a supersonic mixing layer interacting with an oblique shock wave is investigated analytically and numerically under conditions such that the post-shock flow remains supersonic. The study requires consideration of the structure of the post-shock ignition kernel that is found to exist around the point of maximum temperature, which may be located either near the edge of the mixing layer or in its interior, depending on the profiles of the fuel concentration, temperature, and Mach number across the mixing layer. The ignition kernel displays a balance between the rates of chemical reaction and of post-shock flow expansion, including the acoustic interactions of the chemical heat release with the shock wave, leading to increased front curvature. The analysis, which adopts a one-step chemistry model with large activation energy, indicates that ignition develops as a fold bifurcation, the turning point in the diagram of the peak perturbation induced by the chemical reaction as a function of the Damköhler number providing the critical conditions for ignition. While an explicit formula for the critical Damköhler number for ignition is derived when ignition occurs in the interior of the mixing layer, under which condition the ignition kernel is narrow in the streamwise direction, numerical integration is required for determining ignition when it occurs at the edge, under which condition the kernel is no longer slender. Subsequent to ignition, for the Arrhenius chemistry addressed, the lead shock will rapidly be transformed into a thin detonation on the fuel side of the ignition kernel, and, under suitable conditions, a deflagration may extend far downstream, along with the diffusion flame that must separate the rich and lean reaction products. The results can be helpful in describing supersonic combustion for high-speed propulsion.

Key Words: mixing layer, shock waves, ignition theory, supersonic combustion

1. Introduction

The design of nonpremixed-combustion systems for supersonic propulsion faces difficulties associated with the high flow velocity, which limits the residence time available for completion of the chemical reaction in the combustion chamber. Since flame propagation is precluded by the flow velocities needed in these applications, combustion stabilization must rely on autoignition of the fuel-air mixture. The autoignition times of most fuel-air mixtures are strongly dependent on the temperature, with the consequence that the resulting autoignition distance is very sensitive to the existing boundary conditions. In

† Email address for correspondence: als@ucsd.edu

supersonic combustion, autoignition is facilitated by the elevated temperature found in the air stream and also by the added internal heating associated with viscous dissipation acting in the highly strained mixing layers separating the air and fuel streams. Local compression by shock waves impinging on mixing layers also promotes autoignition in nonpremixed systems by raising the temperature of the shocked gas, which is the phenomenon addressed in this paper. Ignition triggering by shock-wave impingement is of particular relevance for propulsion systems employing hydrocarbon fuels because their associated autoignition times are considerably larger than those of more reactive fuels, such as hydrogen, thereby placing more stringent constraints on the completion of the combustion process in the available residence time.

The compressible flow found in the combustion chambers of supersonic-combustion ramjets (SCRAMJETS) often involves oblique shocks, formed in the combustor by interactions of the air stream with wedged walls and fuel injectors. Although these shock waves are generally undesirable for an efficient operation of propulsion systems in that they induce total-pressure loss, their interaction with the mixing layers that separate the fuel and air streams was shown by Marble et al. (1987) to have a beneficial effect on the overall combustion efficiency by increasing the reactant mixing rate. This aspect of the shock/mixing-layer interaction process has been examined in the past in non-reacting flows (Menon 1989; Lu & Wu 1991; Marble 1994; Nuding 1996; Brummund & Nuding 1997; Génin & Menon 2010; Zhang et al. 2015). By way of contrast, the enhancement of the chemical reaction by shock heating and the conditions needed to achieve ignition in this interacting compressible-flow configuration do not seem to have been analyzed in earlier work.

Although the prevailing conditions are turbulent in the high-Reynolds-number flows present in supersonic-combustion chambers, a laminar flow configuration is investigated in this initial study of shock-induced ignition in supersonic mixing layers as a necessary preliminary step in developing understanding of the nontrivial thermo-acoustic interactions that determine the occurrence of ignition in these systems. Specifically, we consider a laminar mixing layer separating supersonic parallel streams of air and fuel moving at different velocities. An oblique shock wave generated on the air side, with initial incident angle σ_∞, impinges on the mixing layer at a given downstream location, as shown in the schematic view of figure 1, where the air stream is located on the upper side. The general layout, including the consideration of a shock wave originated on the air side, is motivated by observed interactions between oblique shocks and mixing-layer flows in SCRAMJET combustors; see, for instance, figures 5 and 11 of Waidmann et al. (1994) and figure 4 of Laurence et al. (2013).

Previous work relevant to our analysis falls into two major categories, namely, studies of autoignition processes leading to diffusion-flame formation in laminar mixing layers free from shock impingement and studies of chemically frozen interactions of shocks with laminar mixing layers. The former problem was addressed in the seminal asymptotic analysis of Liñán & Crespo (1976), who identified the key competing physicochemical phenomena and delineated the parametric dependences of the different ignition regimes for systems with a strong temperature dependence of the chemical reaction rate. In particular, they found that in configurations where one of the streams is significantly hotter than the other (the air being hotter in most propulsion applications), the chemical reaction is confined to a concentrated region near the hot side of the mixing layer. The analysis, including effects of nonnegligible consumption of the deficient reactant, identifies a hot-side reactive-diffusive ignition kernel that determines the critical ignition distance. In supersonic mixing layers, however, the ignition-kernel structure may differ, and, moreover, the peak temperature is not always on the air side; although the air is hotter than

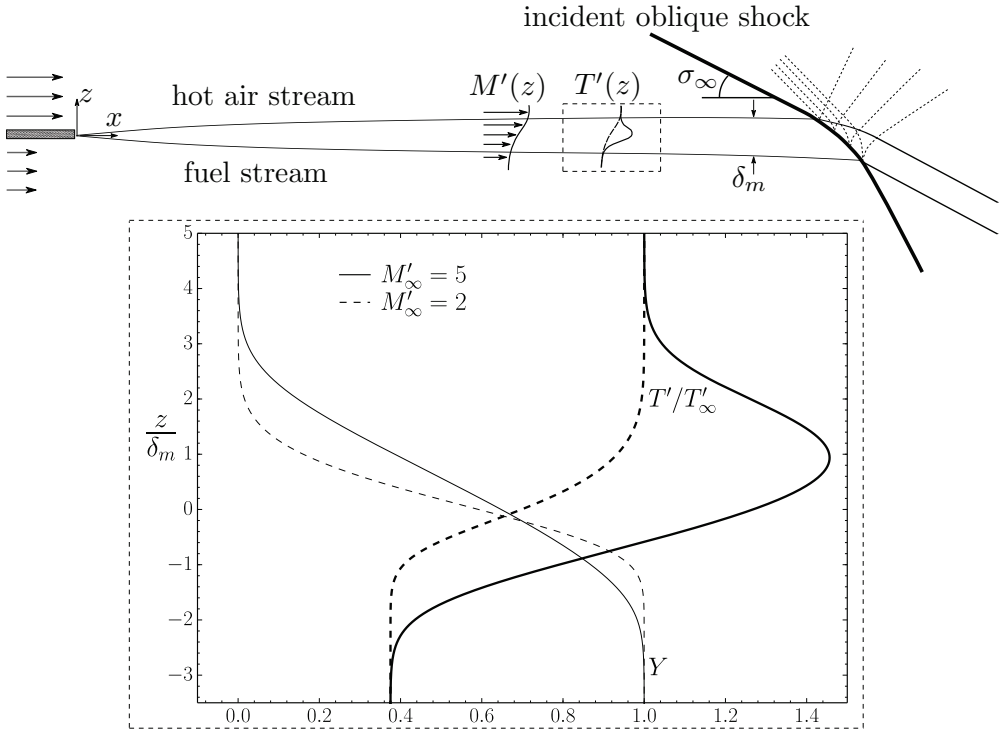

FIGURE 1. Sketch of the mixing-layer/shock-wave configuration investigated. The blowup shows upstream mixing-layer profiles of temperature (thick curves) and fuel mass fraction (thin curves) obtained with $M'_{-\infty} = 1.5$ and $T'_{-\infty}/T'_\infty = 0.375$ for $M'_\infty = 2.0$ (dashed curves) and $M'_\infty = 5.0$ (solid curves), with $\delta_m = 2[D_F x/U'_\infty]^{1/2}$ representing the mixing-layer thickness, computed at a given downstream location x with use made of the fuel diffusivity D_F and airstream velocity U'_∞; see (Huete et al. 2015) for details of the associated computations.

the fuel, the temperature profile may develop a maximum at an intermediate location as a result of the effect of viscous dissipation when the existing shear is sufficiently high and the temperature difference between the two streams is not too pronounced.

These temperature-profile modifications are illustrated in figure 1, which shows self-similar profiles of temperature and fuel mass fraction determined numerically for a mixing layer with fuel-side Mach number $M'_{-\infty} = 1.5$ and fuel-to-air temperature ratio $T'_{-\infty}/T'_\infty = 0.375$ for two different values of the airstream Mach number M'_∞. These sample integrations including viscous dissipation neglect variations of the mean molecular weight and assume a fuel Lewis number of unity, with thermal diffusion neglected, as is appropriate for fuels that have properties close to those of air, such as ethylene, which has been employed in recent supersonic-combustion research (Dolvin 2008). A detailed description of the mixing-layer formulation employed in the integrations can be found in Huete et al. (2015).

As can be seen in figure 1, for the temperature ratio $T'_{-\infty}/T'_\infty = 0.375$ considered the heating associated with viscous dissipation when $M'_\infty = 2$ is not sufficiently intense to promote the appearance of a local maximum inside the mixing layer, so that the temperature profile remains monotonic. For this case, therefore, autoignition would tend to occur near the air boundary, as described by Liñán & Crespo (1976). The temperature monotonicity disappears as shear is increased above a given threshold value, as can be

seen in the results for $M'_\infty = 5$, which exhibit a pronounced maximum in the temperature profile at an intermediate location in the mixing layer. This has a significant effect on the resulting ignition distance, as noted by Jackson & Hussaini (1988) and Grosch & Jackson (1991). The ignition kernel moves to the location of maximum temperature, where the concentrations of both reactants are comparable with those found in their respective feed streams, so that the incipient chemical reaction can be described with effects of reactant consumption neglected in the first approximation, giving rise to a different ignition regime than that associated with a monotonic temperature profile. All of these early analytical studies of ignition, aimed at developing fundamental knowledge, employed a one-step Arrhenius model with large activation energy for the chemical reaction, thereby enabling analytical results to be developed. Our analysis below is based on this same chemistry. More realistic chemistry descriptions have been employed in later work on mixing-layer ignition, in particular in connection with hydrogen-air systems, as reviewed by Sánchez & Williams (2014).

Concerning the second type of investigation relevant to our work, namely nonreacting shock interactions with nonuniform streams, a fundamental contribution to the understanding of the interplay of an oblique shock and a chemically frozen laminar shear layer is the pioneering study of Moeckel (1952), who described the acoustic interactions occurring behind the shock in an ideal gas with constant heat capacities when the post-shock flow remains supersonic everywhere. By neglecting the effect of the pressure waves reaching the shock from behind, he was able to derive an approximate analytical method to determine the shape of the curved shock front in terms of the nonuniform Mach-number distribution across the mixing layer. His method was later generalized by Whitham (1958) to other shock-wave problems and was more recently used by Buttsworth (1996) as a basis to describe the supersonic vorticity field in shocked mixing layers with the objective of assessing mixing augmentation (note that this last author seems to have been unaware of the previous work). These analyses of shock/mixing-layer interactions pertained to supersonic mixing layers subjected to oblique shocks with incident angles sufficiently small for the post-shock flow to remain supersonic all across the mixing layer. Moeckel's method is no longer applicable when incident-flow conditions are reached such that the shocked gas becomes subsonic, because the character of the problem then changes from hyperbolic to elliptic, involving acoustic coupling of the flow with the shock wave in the subsonic region.

The shock/mixing-layer interaction leads to a much more complicated flow structure when the low-velocity stream is subsonic, the shock wave approaching the mixing layer from the supersonic side. In that case, the perturbations generated by the shock-wave impingement propagate upstream on the subsonic side, altering significantly the flow and deflecting the incoming mixing layer. Previous investigations of the resulting shock-reflection problem have been restricted to weak shocks (Riley 1960; Huete et al. 2015), including upstream perturbations of small amplitude, a case for which the theory of shock/boundary-layer interaction developed by Lighthill (1950, 1953) was found to be instrumental in deriving analytical results. The interaction of transonic mixing layers with shocks of finite strength, including significant perturbations on the subsonic side upstream from the shock, appears to be a difficult problem not treated previously, in which the unknown location of the shock wave is coupled with the mixing-layer deflection. This problem deserves attention in the future.

In the limit of large activation energy, describing the strong temperature sensitivity of the heat-release rate present in most fuels, the solution in the ignition regime is in the first approximation that corresponding to the chemically frozen problem, which is described in § 2. The Euler equations are formulated there in characteristic form, which helps to

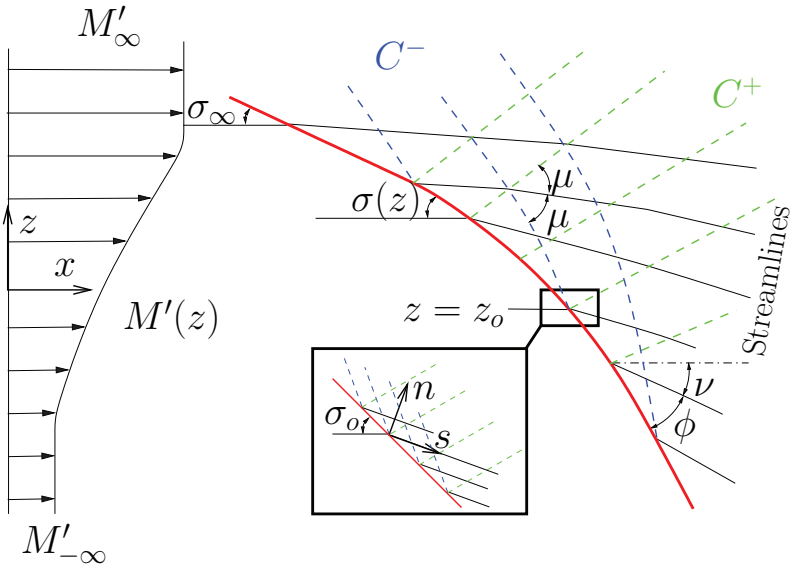

FIGURE 2. A schematic view of the characteristic curves in the post-shock flow; the inset shows the local coordinate system used for the description of the ignition kernel.

clarify the acoustic interactions occurring in the post-shock flow, including their influence on the shock curvature. We shall show that, under most but not all conditions, the flow behind the curved front undergoes an expansion that cools the gas downstream from the shock. As a result of the induced temperature decrease, the conditions most favorable for ignition are found immediately behind the shock, in a region around the peak temperature of the shocked gas. The thickness of this region, which is small compared with the mixing-layer thickness for large activation energies, is determined by the post-shock expansion rate. Since the ignition region is small, when describing the weakly reactive flow in the ignition kernel, the reactive Euler equations can be linearized following the standard Frank-Kamenetskii (1969) approach, providing the formulation given in § 3. The two regimes identified in figure 1 will be seen to require separate analyses, which are given in § 4 for ignition inside the mixing layer at a temperature maximum and in § 5 for ignition near the air boundary. The post-ignition development of the heat-release profiles is described in § 6, where relationships to detonations are addressed. Finally, concluding remarks are given in § 7.

2. The interaction of an oblique shock with a supersonic mixing layer

In the following analysis, cartesian coordinates (x, z) will be used to describe the mixing layer, with x aligned with the unperturbed flow and z being the corresponding transverse coordinate, as indicated in figure 2. Except for the fuel mass fraction Y, which does not change across the shock, a prime $'$ will be used to denote properties in the unperturbed flow upstream from the shock wave, while unprimed symbols will be used for the flow properties in the post-shock region. Besides the pressure $p' = p'_\infty$, which is uniform, the mixing layer is defined by the transverse distributions of fuel mass fraction $Y(z)$, Mach number $M'(z)$ and temperature $T'(z)$, which evolve from the values found in the air stream $Y(\infty) = 0$, $M'(\infty) = M'_\infty$ and $T'(\infty) = T'_\infty$ to reach the values $Y(-\infty) = 1$, $M'(-\infty) = M'_{-\infty}$ and $T'(-\infty) = T'_{-\infty}$ in the fuel stream, with $M'_{-\infty} < M'_\infty$ and

$T'_{-\infty} < T'_{\infty}$ in typical applications. As previously mentioned, while the Mach number normally decreases monotonically with the distance from the air boundary, depending on the extent of viscous-dissipation heating, the maximum of the temperature profile may be reached either on the air side or at an intermediate location inside the mixing layer, leading to two different shock-induced-ignition scenarios that are analyzed separately below.

The interaction of the shock with the mixing layer results in a complicated free-boundary problem in which the shape of the curved shock front, defined by the incident angle $\sigma(z)$, is coupled to the post-shock flow. The solution requires integration of the Euler equations downstream from the shock. At the shock, the different properties can be evaluated in terms of σ and M' for a given value of the specific-heat ratio γ by use of the Rankine-Hugoniot relations, including the jumps of temperature and pressure,

$$\frac{T}{T'} = F_T(M', \sigma) = \frac{[2\gamma M'^2 \sin^2\sigma + 1 - \gamma][(\gamma - 1)M'^2 \sin^2\sigma + 2]}{(\gamma + 1)^2 M'^2 \sin^2\sigma}, \tag{2.1}$$

$$\frac{p}{p'_{\infty}} = F_p(M', \sigma) = \frac{2\gamma M'^2 \sin^2\sigma + 1 - \gamma}{\gamma + 1}, \tag{2.2}$$

the clockwise flow deflection

$$\nu = F_\nu(M', \sigma) = \tan^{-1}\left\{\frac{2(M'^2 \sin^2\sigma - 1)\cot\sigma}{2 + M'^2[\gamma + \cos(2\sigma)]}\right\}, \tag{2.3}$$

and the post-shock Mach number

$$M = \frac{1}{\sin\phi}\left[\frac{2 + (\gamma - 1)M'^2 \sin^2\sigma}{2\gamma M'^2 \sin^2\sigma + 1 - \gamma}\right]^{1/2}, \tag{2.4}$$

where $\phi = \sigma - \nu$. For a given value of $M' > 1$, there exists a critical value of σ that renders the post-shock flow sonic, to be calculated from (2.3) and (2.4) with $M = 1$. The resulting boundary line $\sigma(M')$ is plotted in figure 3 for $\gamma = 1.4$ and $\gamma = 1.2$, selected as limiting representative values characterizing the conditions found in typical applications. The figure also shows the lower boundary value $\sigma = \sin^{-1}(1/M')$ corresponding to infinitesimally weak shocks, along with other curves, to be discussed later.

The solution simplifies when the post-shock flow remains supersonic, that being the case considered in the present analysis. The Euler equations can be formulated in characteristic form, with three different characteristic lines crossing any given point, i.e., the streamline and the two Mach lines, with different characteristic equations applying along each of them. The corresponding form of the equations is given below for chemically frozen flow. The modified equations that describe the ignition problem are to be presented in the next section.

In the absence of chemical reaction, the entropy is conserved along the streamlines, a condition that can be expressed in the form

$$\frac{\mathrm{d}T}{T} - \frac{\gamma - 1}{\gamma}\frac{\mathrm{d}p}{p} = 0, \quad \text{on} \quad \frac{\mathrm{d}z}{\mathrm{d}x} = \tan\lambda, \tag{2.5}$$

where λ is the (counterclockwise) local angle of deflection of the streamlines with respect to the horizontal. On the other hand, manipulation of the conservation equations of continuity and momentum provides two additional characteristic equations, each corresponding to one of the Mach lines. In terms of p and λ the equations read (Hayes & Probstein

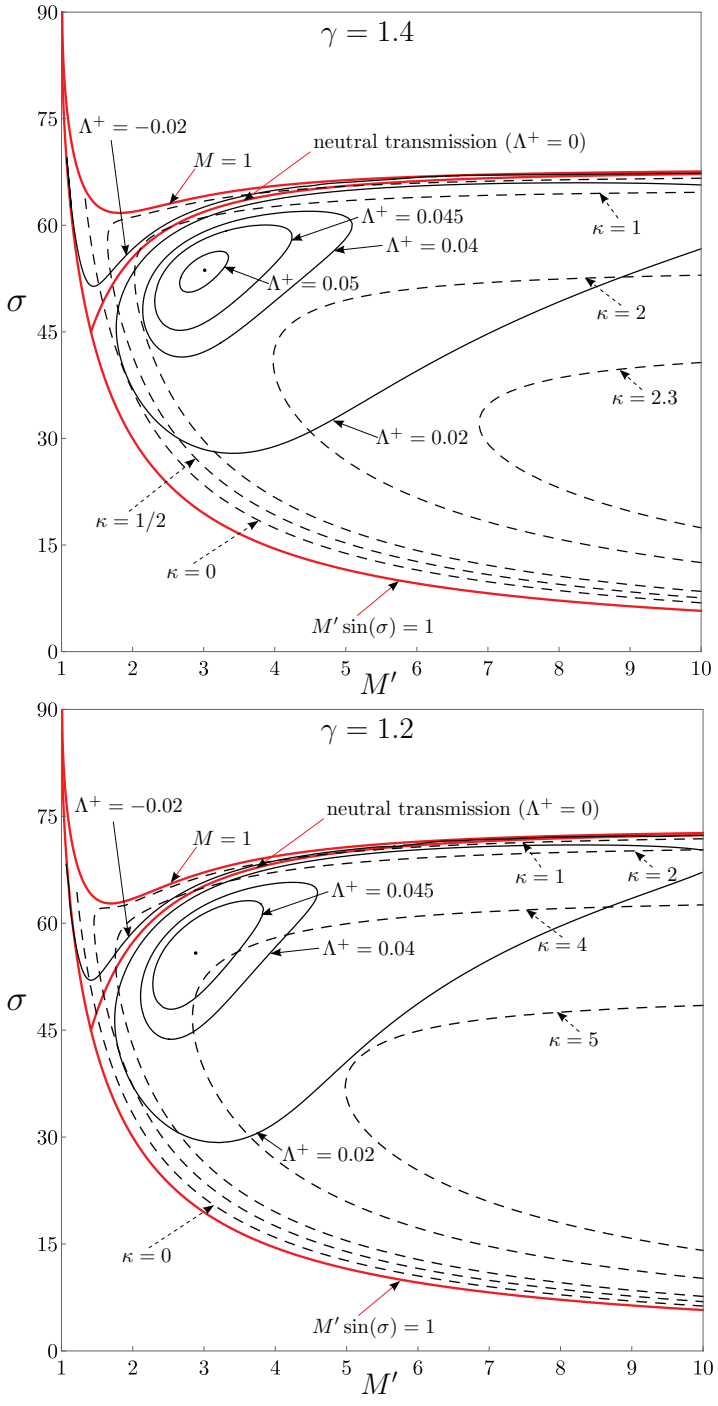

FIGURE 3. The three red curves represent the limiting values of σ corresponding to an infinitesimally weak shock, neutral oblique-shock transmission, and sonic post-shock conditions. The black curves represent isolines of the function Λ^+ defined in (4.8) (solid curves) and of the function κ defined in (4.19) (dashed curves). The upper and lower plots correspond to results for $\gamma = 1.4$ and for $\gamma = 1.2$, respectively.

2004)

$$\frac{\mathrm{d}p}{p} \pm \frac{\gamma M^2}{\sqrt{M^2-1}}\mathrm{d}\lambda = 0, \quad \text{on} \quad \frac{\mathrm{d}z}{\mathrm{d}x} = \tan(\lambda \pm \mu), \tag{2.6}$$

where

$$\mu = \sin^{-1}\left(\frac{1}{M}\right) \tag{2.7}$$

is the angle of inclination of the two Mach lines relative to the local flow direction, as depicted in figure 2. The integration along the streamlines and along the C^+ characteristic lines $\mathrm{d}z/\mathrm{d}x = \tan(\lambda+\mu)$ starts at the shock, with corresponding initial conditions evaluated from the Rankine-Hugoniot relations given above (e.g., $\lambda = -\nu$ at the shock). On the other hand, the C^- characteristics originate in the shocked air stream above the mixing layer, so that the associated uniform values of p_∞ ($> p'_\infty$) and $\lambda_\infty = -\nu_\infty$ must be used as initial conditions in the integration, which must be continued until the C^- characteristic line intersects the shock, providing the information needed at each point to determine the shock curvature $\mathrm{d}\sigma/\mathrm{d}z$. As a consequence of the existence of the C^- characteristics reaching the shock from above, the value of $\sigma(z)$ at a given height z^*, which depends on the local value of $M'(z^*)$ through the Rankine-Hugoniot relations, depends also on the distribution of $T'(z)$ and $M'(z)$ for $z > z^*$, because they determine the nonuniform field along the C^- characteristic intersecting the shock at $z = z^*$.

Clearly, therefore, even in the chemically frozen case, the determination of the shock-front shape $\sigma(z)$ is a complicated non-local problem that requires numerical integration. To the best of our knowledge, such a computation has not been attempted yet. The complexity of the associated calculation was acknowledged in the early work of Moeckel (1952), who developed an approximate analytic method for determining the shock shape $\sigma(z)$ in which the waves generated at the shock by the shock-flow interaction process are taken into account, while the waves originated by internal reflection in the nonuniform post-shock region are entirely neglected. As explained by Whitham (1958), Moeckel's method amounts to applying the relation $\mathrm{d}p/p = \gamma M^2 \mathrm{d}\lambda/\sqrt{M^2-1}$, corresponding to the C^- characteristic line, along the shock front, thereby yielding

$$\frac{\mathrm{d}p}{p} = -\frac{\gamma M^2}{\sqrt{M^2-1}}\mathrm{d}\nu. \tag{2.8}$$

Using

$$\frac{\mathrm{d}p}{p} = A_p \mathrm{d}M' + B_p \mathrm{d}\sigma \tag{2.9}$$

and

$$\mathrm{d}\nu = A_\nu \mathrm{d}M' + B_\nu \mathrm{d}\sigma \tag{2.10}$$

in (2.8) finally provides

$$\frac{\mathrm{d}\sigma}{\mathrm{d}M'} = -\frac{A_p + \gamma M^2 A_\nu/(M^2-1)^{1/2}}{B_p + \gamma M^2 B_\nu/(M^2-1)^{1/2}}, \tag{2.11}$$

as a local expression for the shock curvature, where

$$A_p = \frac{1}{F_p}\frac{\partial F_p}{\partial M'}, \quad B_p = \frac{1}{F_p}\frac{\partial F_p}{\partial \sigma}, \quad A_\nu = \frac{\partial F_\nu}{\partial M'}, \quad B_\nu = \frac{\partial F_\nu}{\partial \sigma} \tag{2.12}$$

can be evaluated explicitly in terms of σ and M' from the Rankine-Hugoniot relations (2.2) and (2.3). In Moeckel's simplified approach, integration of (2.11) with initial

condition $\sigma = \sigma_\infty$ at $M' = M'_\infty$ provides $\sigma(M')$, thereby determining $\sigma(z)$ for a given upstream Mach-number distribution $M'(z)$.

For the following ignition analysis, it is of interest to note that, under most conditions, the C^+ characteristic lines issuing from the shock represent an expansion wave that reduces the pressure (and therefore the temperature) along the streamlines downstream from the shock. The prevalence of expansion waves can be demonstrated by identifying the upstream conditions under which neutral oblique-shock transmission is achieved (i.e., the post-shock flow is neither expanded nor compressed locally). If the effect of the downstream disturbances on the shock is neglected, following the approximation adopted by Moeckel (1952), then the condition for neutral transmission is that $\mathrm{d}p = \mathrm{d}\nu = 0$, with $\mathrm{d}p$ and $\mathrm{d}\nu$ given in (2.9) and (2.10). The associated curve of neutral transmission

$$\sin^2\sigma = \frac{\gamma+1}{2\gamma} - \frac{1}{\gamma M'^2}, \tag{2.13}$$

derived by using (2.2) and (2.3) to evaluate the coefficients (2.12) in (2.9) and (2.10), is plotted figure 3. A compression appears in the post-shock flow when the value of σ is larger than the neutral-transmission value, a criterion satisfied in a relatively small corner region in the $M' - \sigma$ diagram of figure 3 bounded by the curve of neutral transmission and the limiting curves $M = 1$ and $M' \sin\sigma = 1$. In the absence of the approximation yielding (2.13), identification of the neutral-transmission condition becomes a non-local problem not identifiable as a region in figure 3, but post-shock compression would be expected to be a comparatively rare occurrence in any event. This small parametric region is therefore not considered further hereafter.

Our near-shock ignition analysis pertains instead to conditions that place the system inside the extended parametric region corresponding to values of $\sigma > \sin^{-1}(1/M')$ below the neutral-transmission curve, when the gas downstream from the shock cools down as a result of the expansion, so that the peak temperature is found immediately downstream from the shock. Then, because of the strong temperature sensitivity of the chemical reaction, we find in the vicinity of the shock front a small ignition kernel where the incipient chemical reaction is competing with the flow expansion. Critical conditions for ignition will be determined by examining whether weakly reactive solutions exist in this ignition kernel. It will be found that, if heat-release rates are too large, then such solutions fail to exist, corresponding to ignition having occurred. The analysis will show that, in addition to the existing background wave system of the chemically frozen flow, the ignition event is fundamentally influenced by the additional pressure waves generated by the chemical heat release, which are seen to interact with the shock front, modifying its curvature and the associated jump conditions.

3. Formulation of the weakly reactive problem

Since the chemical reaction displays a strong temperature dependence, ignition occurs near the point $z = z_o$ where the post-shock temperature of the chemically frozen solution reaches its peak value. The local weakly reactive flow can be described as a perturbation to the frozen solution using a cartesian coordinate system that includes the streamwise distance s along the post-shock streamline that departs from $z = z_o$ and the associated transverse coordinate n pointing towards the air side, both scaled with the characteristic mixing-layer thickness δ, to be defined precisely in (4.1), comparable in order of magnitude to the thickness δ_m used to represent the sample profiles shown in figure 1. A sketch indicating the local coordinate system is given in the inset of figure 2, the relevant angles also being indicated on the figure.

3.1. *Linearized weakly reactive equations*

A one-step model will be used for the chemical reaction, with the mass of fuel consumed per unit volume and unit time given in terms of the local fuel mass fraction Y and temperature T by the Arrhenius expression $\tilde{\omega} = \rho Y B \exp(-T_a/T)$, involving the gas density ρ, the frequency factor B, and the activation temperature T_a, which in our analysis is assumed to be large compared with the ignition-kernel temperature. The expression adopted for the reaction rate assumes that the fuel is the limiting reactant in practical applications, while the consumption of the oxidizer has no effect during the ignition stage, so that the local oxidizer mass fraction in the ignition kernel can be conveniently absorbed in the definition of the constant frequency factor B. In this simple model, $\tilde{q}$ represents the amount of heat released per unit mass of fuel burnt. The governing equations for the flow are obtained by linearizing the reactive Euler equations around the post-shock solution found at $z = z_o$, with a Frank-Kamenetskii linearization adopted for the exponential temperature dependence of the reaction rate, as is needed to describe ignition events (Williams 1985). The procedure is identical to that used in classical textbooks (Hayes & Probstein 2004) when deriving characteristic equations for supersonic isentropic flows, with the condition of constancy of entropy replaced in our analysis by the equations describing the chemical heat release along the streamlines. We begin by writing the conservation equations in their primitive form and proceed to derive the characteristic equations, which differ from those given above in (2.5) and (2.6) owing to the presence of the chemical reaction. The linearization will allow us to define characteristic variables $I^{\pm}$ that effectively replace p and λ in the integration along the Mach lines $C^{\pm}$.

The basic state is defined by the local post-shock non-reactive-flow values of the flow deflection, temperature, pressure, Mach number, and streamwise velocity, denoted by $\lambda_o = -\nu_o$, T_o, p_o, M_o, and $U_o = M_o\sqrt{(\gamma-1)c_pT_o}$ at $z = z_o$, with c_p denoting the specific heat at constant pressure. The problem can be formulated in terms of the pressure and temperature perturbations $\bar{p} = (p-p_o)/p_o$ and $\bar{T} = (T-T_o)/T_o$ and the ratio $\bar{V} = V/U_o$ of the transverse velocity V to the unperturbed velocity U_o (i.e., $\bar{V} = \lambda - \lambda_o$ in the linear approximation adopted here). These dimensionless variables can be used to write the streamwise and transverse components of the momentum balance equation in the form

$$\frac{\gamma M_o^2 - 1}{\gamma M_o^2}\frac{\partial \bar{p}}{\partial s} - \frac{\partial \bar{T}}{\partial s} + \frac{\partial \bar{V}}{\partial n} = 0 \tag{3.1}$$

$$\gamma M_o^2 \frac{\partial \bar{V}}{\partial s} + \frac{\partial \bar{p}}{\partial n} = 0, \tag{3.2}$$

after the continuity equation and the equation of state are used to express the perturbations of density and streamwise velocity in terms of $\bar{p}$, $\bar{T}$, and $\bar{V}$. In terms of these variables, the energy and fuel conservation equations become

$$\frac{\partial \bar{T}}{\partial s} - \frac{\gamma - 1}{\gamma}\frac{\partial \bar{p}}{\partial s} = Q\omega \tag{3.3}$$

and

$$\frac{\partial Y}{\partial s} = -\omega, \tag{3.4}$$

where $Q = \tilde{q}/(c_pT_o)$ is a dimensionless chemical heat release and, after the Frank-Kamenetskii linearization $\exp[\beta\bar{T}/(1+\bar{T})] \simeq \exp(\beta\bar{T})$,

$$\omega = \left(\frac{B}{U_o/\delta}\right) e^{-\beta} Y e^{\beta\bar{T}} \tag{3.5}$$

is the nondimensional reaction rate. The dimensionless activation temperature $\beta = T_a/T_o$ is the large parameter for the asymptotic description below.

The problem can be conveniently formulated in characteristic form by combining linearly (3.1)–(3.3) to give

$$\frac{\partial I^{\pm}}{\partial s} \pm \frac{1}{\sqrt{M_o^2 - 1}} \frac{\partial I^{\pm}}{\partial n} = \frac{\gamma M_o^2}{M_o^2 - 1} Q\omega \tag{3.6}$$

for the characteristic variables

$$I^{\pm} = \bar{p} \pm \frac{\gamma M_o^2}{\sqrt{M_o^2 - 1}} \bar{V}, \tag{3.7}$$

which can be used to rewrite (3.3) as

$$\frac{\partial \bar{T}}{\partial s} - \frac{\gamma - 1}{2\gamma} \frac{\partial}{\partial s}(I^+ + I^-) = Q\omega. \tag{3.8}$$

Equations (3.4), (3.6), and (3.8) supplemented with (3.5) are the basis for the local description of thermal ignition events in two-dimensional, steady supersonic flows. Similar linearized equations have been employed in analyses of ignition of a gaseous reactive mixture subject to a localized energy source (Vázquez-Espí & Liñán 2001).

3.2. *Boundary conditions*

As can be inferred from (3.3) and (3.4), the fuel mass fraction Y and the dimensionless entropy perturbation $\bar{T} - (\gamma - 1)\bar{p}/\gamma$ evolve along the streamlines $n =$ constant, while the characteristic variables $I^{\pm}$ are seen in (3.6) to evolve along the Mach lines

$$C^{\pm}: \quad s + \frac{n}{\tan \phi_o} = \left(\frac{1}{\tan \phi_o} \pm \frac{1}{\tan \mu_o} \right) (n - n_s), \tag{3.9}$$

involving the local downstream-flow inclination $\phi_o = \sigma_o - \nu_o$ with respect to the shock. Here, n_s denotes the value of n corresponding to the point where the Mach line intersects the shock, whose location is defined in this linear approximation by the straight line $s + n/\tan \phi_o = 0$. As indicated earlier, since the normal component of the velocity behind the shock is subsonic (i.e., $\mu_o > \phi_o$), the C^- characteristics always reach the shock, while the C^+ characteristics originate there. Therefore, in writing below the boundary conditions for (3.4), (3.6), and (3.8) we need to specify the values of Y, $\bar{T}$, and I^+ at the shock, while the boundary value of I^- along a given C^- characteristic must be specified outside the ignition kernel, thereby introducing appreciable complexity into application of the boundary conditions. A zero boundary value of I^- must be used for all characteristics C^- in analyzing ignition occurring near the air-side edge of the mixing layer to be consistent with the uniform conditions found in the air stream. When ignition occurs inside the mixing layer far from the air boundary, however, a linear distribution $I^- \propto n_s$ must in general be considered instead as indicated below in (4.4), with the proportionality coefficient determined in general from the numerical computation of the chemically frozen flow for $z > z_o$. Note that, if the simplified strategy proposed by Moeckel (1952) is adopted for the base computation of the shock-wave shape, then the resulting boundary value I^- is identically zero everywhere along the shock. In this approximation, which is reasonably accurate under a wide range of conditions as discussed by Moeckel (1952), adoption of the boundary condition $I^- = 0$, strictly valid only for ignition events occurring right at the air boundary, would give reasonably accurate predictions of ignition conditions even when the reactive kernel is located at an intermediate transverse location inside the mixing layer.

The composition does not change across the chemically inert shock, so that the boundary condition for the fuel mass fraction along the shock line $s + n/\tan\phi_o = 0$ can be directly evaluated in terms of the upstream transverse distribution $Y(z)$. Since the heat released in the reaction may perturb the shock, the boundary values of $\bar{T}$ and I^+ are obtained by analyzing the local jumps of temperature, pressure, and velocity across the shock. Linearizing the Rankine-Hugoniot relations (2.1)–(2.3) around the upstream values of the temperature, Mach number, and incident angle T'_o, M'_o, and σ_o at $z = z_o$ yields

$$\bar{T} = \bar{T}' + A_T\bar{M}' + B_T\bar{\sigma}, \quad \bar{p} = A_p\bar{M}' + B_p\bar{\sigma}, \quad \text{and} \quad \bar{V} = -A_\nu\bar{M}' - B_\nu\bar{\sigma}, \tag{3.10}$$

for the post-shock perturbations in terms of $\bar{T}' = (T' - T'_o)/T'_o$, $\bar{M}' = M' - M'_o$, and $\bar{\sigma} = \sigma - \sigma_o$. The coefficients A_p, B_p, A_ν, and B_ν for the pressure and transverse-velocity perturbations, defined above in (2.12), as well as the accompanying coefficients

$$A_T = \frac{1}{F_T}\frac{\partial F_T}{\partial M'} \quad \text{and} \quad B_T = \frac{1}{F_T}\frac{\partial F_T}{\partial \sigma} \tag{3.11}$$

for the temperature perturbations are to be obtained from evaluations of the Rankine-Hugoniot relations (2.1)–(2.3) and their derivatives at $M' = M'_o$ and $\sigma = \sigma_o$. The corresponding post-shock values of the characteristic variables $I^\pm$ are given by

$$I^\pm = A^\pm\bar{M}' + B^\pm\bar{\sigma}, \tag{3.12}$$

with

$$A^\pm = A_p \mp \frac{\gamma M_o^2}{\sqrt{M_o^2 - 1}}A_\nu \quad \text{and} \quad B^\pm = B_p \mp \frac{\gamma M_o^2}{\sqrt{M_o^2 - 1}}B_\nu, \tag{3.13}$$

as follows from the definitions given in (3.7). While the distributions of M' and T' upstream from the shock are independent of the post-shock flow and can be prescribed in the ignition analysis, the local shock curvature $\bar{\sigma}$ depends on the incipient chemical reaction through the value of I^- reaching the shock from above, as can be seen by solving (3.12) for

$$\bar{\sigma} = -\frac{A^-}{B^-}\bar{M}' + \frac{1}{B^-}I^-. \tag{3.14}$$

Using this expression in (3.10) and (3.12) finally yields

$$\bar{T} = \bar{T}' + \left(A_T - \frac{B_T}{B^-}A^-\right)\bar{M}' + \frac{B_T}{B^-}I^- \tag{3.15}$$

and

$$I^+ = \left(A^+ - \frac{B^+}{B^-}A^-\right)\bar{M}' + \frac{B^+}{B^-}I^- \tag{3.16}$$

for the boundary values of $\bar{T}$ and I^+ at the shock. Since the coefficients B_T and B^- are always positive, the increase in I^- associated with the chemical reaction acting along the characteristic C^- results in increasing values of the shock curvature and post-shock temperature, as dictated by (3.14) and (3.15).

4. Ignition at a local temperature maximum

We consider first ignition events occurring when the peak temperature T_o of the nonreacting shocked gas occurs at an intermediate location z_o across the mixing layer, that being the case when the associated upstream temperature profile $T'(z)$ displays a maximum across the mixing layer as a result of viscous dissipation, as occurs for $M'_\infty = 5$ in the

computations of figure 1. Note that, since the temperature of the shocked gas depends also on the variation of M', the resulting transverse location z_o is slightly displaced upwards with respect to the location where $T'(z)$ reaches its peak value. Observation of (3.5) reveals that the ignition regime corresponds to small temperature increments $\bar{T} = (T - T_o)/T_o \sim \beta^{-1} \ll 1$, as required to increase the chemical-reaction rate by an amount of order unity. These temperature increments are associated with small fuel-mass-fraction decrements $Y_o - Y \sim \beta^{-1} \ll 1$. Since the fuel mass fraction $Y = Y_o$ at $z = z_o$ is of order unity, in analyzing ignition the chemical reaction rate (3.5) can be evaluated with use made of the unperturbed fuel mass fraction Y_o, thereby circumventing the need to integrate (3.4). The associated errors, of order β^{-1}, are comparable to those introduced by the Frank-Kamenetskii linearization employed in writing (3.5). The problem therefore reduces to that of integrating (3.6) and (3.8) for a given boundary distribution of I^- for $s > -n/\tan\phi_o$ and $n \gg 1$, with the boundary values of $\bar{T}$ and I^+ at the shock $s + n/\tan\phi_o = 0$ evaluated with use made of (3.15) and (3.16).

In writing the boundary conditions below, to achieve a maximum simplification we shall employ

$$\delta = \frac{\sin\phi_o}{\sin\sigma_o}\left(\frac{\mathrm{d}M'}{\mathrm{d}z}\right)^{-1}_{z=z_o}, \tag{4.1}$$

as a definition for the mixing-layer thickness, thereby reducing the local upstream Mach-number distribution to

$$\bar{M}' = n_s, \tag{4.2}$$

where $n_s = (\sin\phi_o/\sin\sigma_o)(z - z_o)/\delta$ identifies a given point along the shock wave. Correspondingly, the chemically frozen temperature distribution immediately behind the shock, which peaks at $n_s = 0$, can be expressed as

$$\bar{T} = -\bar{\Gamma}_T n_s^2, \tag{4.3}$$

where $\bar{\Gamma}_T$ is a measure of the local curvature of the temperature profile. In the linear approximation, the boundary condition for the C^- characteristic equation can be stated in terms of the far-field value

$$I^- = \Gamma^- n_s \tag{4.4}$$

of the characteristic variable I^- along the Mach line C^- that intersects the shock at $n = n_s$, where the factor Γ^- depends on the chemically frozen interactions of the primary isentropic waves with the post-shock Mach-number gradients outside the ignition kernel.

In the following ignition analysis, the coefficients $\bar{\Gamma}_T$ and Γ^- in (4.3) and (4.4) will be assumed to be known order-unity quantities, which must obtained *a priori* for a specific mixing-layer/shock-wave configuration as part of the chemically frozen numerical computation of the shock-wave shape for $z > z_o$, a non-trivial computational problem in general which, however, is simplified if Moeckel's approximation is employed. Although the assumed ordering in principle could be violated if, for example, the temperature profile in the inert mixing layer were extremely sharply peaked, the present ordering applies in the vast majority of realistic cases. Fortunately, moreover, the value of $\bar{\Gamma}_T$ will be seen to be inconsequential for the analysis, in that the critical ignition condition at leading order is independent of the slow boundary variation displayed in (4.3). In addition, although Γ^- does influence the base pressure gradient along the streamlines, which is given later in (4.8), its value can be expected to be moderately small in many situations (if Moeckel's approximation is used in the shock-wave calculation, then $\Gamma^- = 0$).

4.1. *Frozen flow behind the shock*

To identify the scales of the ignition kernel, it is convenient to determine first the temperature distribution found behind the shock when the flow is chemically frozen. Setting $\omega = 0$ in (3.6) and integrating yields $I_F^{\pm}$ along the Mach lines (3.9), where the subscript F is used to denote the chemically frozen variables. Using the shock boundary value (4.4) for I_F^- and the accompanying boundary value

$$I_F^+/n_s = \left(A^+ - \frac{B^+}{B^-}A^-\right) + \frac{B^+}{B^-}\Gamma^- \tag{4.5}$$

evaluated from (3.16) yields the distributions

$$I_F^- = -\Gamma^- \frac{n + s\tan\mu_o}{\tan\mu_o/\tan\phi_o - 1} \tag{4.6}$$

$$I_F^+ = \left(A^+ - \frac{B^+}{B^-}A^- + \frac{B^+}{B^-}\Gamma^-\right)\frac{n - s\tan\mu_o}{\tan\mu_o/\tan\phi_o + 1}, \tag{4.7}$$

which can be used to compute the pressure $\bar{p}_F = (I_F^+ + I_F^-)/2$ and its associated constant streamwise gradient

$$\begin{aligned} -\frac{\partial\bar{p}_F}{\partial s} = \Lambda =& \frac{\tan\mu_o}{2}\left[\frac{A^+ - (B^+/B^-)A^-}{\tan\mu_o/\tan\phi_o + 1}\right] \\ &+ \frac{\tan\mu_o}{2}\left[\frac{B^+/B^-}{\tan\mu_o/\tan\phi_o + 1} + \frac{1}{\tan\mu_o/\tan\phi_o - 1}\right]\Gamma^-. \end{aligned} \tag{4.8}$$

This pressure gradient appears in (3.8), causing the temperature to vary along the streamlines according to

$$\bar{T}_F = -\bar{\Gamma}_T n^2 - \frac{\gamma - 1}{\gamma}\Lambda\left(s + \frac{n}{\tan\phi_o}\right) \tag{4.9}$$

obtained by integrating (3.8) with $\omega = 0$, where $s + n/\tan\phi_o$ is the distance from the shock measured along a streamline $n =$ constant.

The first term in (4.8),

$$\Lambda^+ = \frac{\tan\mu_o}{2}\left[\frac{A^+ - (B^+/B^-)A^-}{\tan\mu_o/\tan\phi_o + 1}\right], \tag{4.10}$$

a function of the local values of the incident Mach number M_o' and incident angle σ_o, corresponds to the intrinsic expansion emanating from the curved shock, whereas the second term

$$\Lambda^- = \frac{\tan\mu_o}{2}\left(\frac{B^+/B^-}{\tan\mu_o/\tan\phi_o + 1} + \frac{1}{\tan\mu_o/\tan\phi_o - 1}\right)\Gamma^- \tag{4.11}$$

accounts for the influence of the external acoustic field transmitted along the C^- Mach lines. As previously noted, Λ^- vanishes for conditions under which the magnitude of the secondary waves induced in the nonuniform flow downstream from the shock is negligibly small. Under most conditions of interest, its associated contribution to Λ, which may reinforce or attenuate the expansion rate depending on its sign, is anticipated to have a lesser quantitative effect, in agreement with Moeckel's postulate.

Isocurves of Λ^+, which vanishes for the conditions of neutral transmission indicated in (2.13), are shown in figure 3. The ignition analysis given below pertains to cases with $\Lambda > 0$, the prevailing conditions below the neutral-transmission curve provided that Λ^- remains moderately small. In the small corner regions of the figure, previously indicated

to be excluded because of their lack of appreciable practical interest, the negative value of Λ implies that the pressure and the temperature actually increase with distance from the shock in the frozen flow, thereby not competing with the chemical heat release.

4.2. *Ignition analysis for $\beta \gg 1$*

In the limit of large activation temperature $\beta \gg 1$ considered here the perturbations associated with the chemical reaction can be described by introducing the rescaled variables $\theta = \beta(\bar{T} - \bar{T}_F)$ and $J^{\pm} = \beta(I^{\pm} - I_F^{\pm})$. According to (4.9), the ignition kernel, where the temperature departs from its peak value by an amount of order $\bar{T} \sim \beta^{-1}$, extends over streamwise distances of order $s + n/\tan\phi_o \sim \beta^{-1}$ and transverse distances of order $n \sim \beta^{-1/2}$, suggesting the introduction of the stretched coordinates

$$\xi = \frac{\gamma - 1}{\gamma}\Lambda\beta\left(s + \frac{n}{\tan\phi_o}\right) \quad \text{and} \quad \eta = \bar{\Gamma}_T^{1/2}\beta^{1/2}n \tag{4.12}$$

for the description of the ignition kernel. The above scaling indicates that in the limit $\beta \gg 1$ the ignition kernel is thin in the streamwise direction provided that the base temperature profile is not extremely sharply peaked, i.e., for values of $\bar{\Gamma}_T$ such that $\bar{\Gamma}_T^{1/2} \ll \Lambda\beta^{1/2}$. These rescaled variables reduce (3.6) and (3.8) to

$$\left(1 \pm \frac{\tan\mu_o}{\tan\phi_o}\right)\frac{\partial J^{\pm}}{\partial\xi} \pm \frac{\gamma\bar{\Gamma}_T^{1/2}\tan\mu_o}{(\gamma-1)\Lambda\beta^{1/2}}\frac{\partial J^{\pm}}{\partial\eta} = \gamma(\tan^2\mu_o + 1)\mathcal{D}e^{-\eta^2-\xi}e^{\theta} \tag{4.13}$$

$$\frac{\partial\theta}{\partial\xi} = \mathcal{D}e^{-\eta^2-\xi}e^{\theta} + \frac{\gamma-1}{2\gamma}\frac{\partial}{\partial\xi}(J^+ + J^-), \tag{4.14}$$

where

$$\mathcal{D} = \frac{\gamma QBY_o e^{-\beta}}{(\gamma-1)\Lambda U_o/\delta} \tag{4.15}$$

is the relevant ignition Damköhler number, defined as the ratio of the characteristic residence time $\gamma\delta/[(\gamma-1)\Lambda\beta U_o]$ required for the temperature to decrease due to the effect of the post-shock gas expansion by a relative amount of order β^{-1} to the characteristic chemical time $[\beta QBY_o e^{-\beta}]^{-1}$ required to increase the temperature as a result of the chemical heat release by that same relative amount. As can be seen in (4.13), in the stretched coordinates the Mach lines (3.9) become

$$C^{\pm}: \quad \xi - \frac{(\gamma-1)\Lambda\beta^{1/2}}{\gamma\bar{\Gamma}_T^{1/2}}\left(\frac{1}{\tan\phi_o} \pm \frac{1}{\tan\mu_o}\right)\eta = \text{constant}. \tag{4.16}$$

The integration along the C^- characteristics must be initiated with the boundary value

$$J^- = 0. \tag{4.17}$$

On the other hand, the boundary conditions for the reactive perturbations at the shock front $\xi = 0$ are given by

$$\theta = \frac{B_T}{B^+}J^+ = \frac{B_T}{B^-}J^-, \tag{4.18}$$

as follows from the linearized Rankine-Hugoniot relations (3.15) and (3.16), since $\bar{T}'$ as well as $\bar{M}'$ and its coefficients are all determined by the unperturbed flow, unaffected by the heat release, as previously demonstrated.

The integration of (4.13) and (4.14) subject to the boundary conditions (4.17) and (4.18) determines the weakly reactive flow in the ignition kernel, including the temperature distribution $\theta = \theta_s(\eta)$ immediately behind the shock. It is worth noting that the value of J^-

at $\xi = 0$, determined by integrating (4.13) across the ignition kernel, is always positive, indicative of a compression wave, which increases the shock-front curvature as it interacts with the shock, as dictated by (3.14), thereby strengthening the shock and resulting in an augmented post-shock temperature $\theta_s > 0$, as can be seen in (4.18) since B_T/B^- is always positive. Equation (4.14) describes the subsequent evolution of the temperature perturbation along the streamlines resulting from the heat released by the chemical reaction, which has a twofold effect. The first term on the right-hand side of (4.14) represents the direct effect of the local heat release rate, which tends to increase the temperature, whereas the second term represents the expansion induced by the chemical reaction, a nonlocal effect that tends to reduce the temperature. As seen below, these two counteracting effects have comparable magnitude, leading to downstream temperature gradients that can be either positive or negative depending on the upstream conditions, as measured by the parameter κ defined later in (4.19).

4.3. *Leading-order solution*

The problem can be solved analytically for large values of the nondimensional activation energy $\beta \gg 1$, because the transverse derivatives in (4.13) become negligible in the first approximation (i.e., the Mach lines (4.16) simplify to $\eta =$ constant), thereby reducing the leading-order problem to the integration of a set of ordinary differential equations in the coordinate ξ. The solution is facilitated by replacing the variables J^- and J^+ by the normalized characteristic variable $\tilde{J} = (B_T/B^-)J^-$ and the pressure perturbation $\pi = \beta(\bar{p} - \bar{p}_F) = (J^- + J^+)/2$. Eliminating the induced streamwise pressure gradient in (4.14) by linear combinations with (4.13) and defining the parameters

$$\kappa = \frac{B^-}{\gamma B_T}\frac{\tan\mu_o/\tan\phi_o - 1}{\tan^2\mu_o + 1}\left[1 - \frac{(\gamma-1)(\tan^2\mu_o+1)}{(\tan\mu_o/\tan\phi_o)^2 - 1}\right], \tag{4.19}$$

and

$$\Delta = \frac{\gamma B_T}{B^-}\frac{\tan^2\mu_o + 1}{\tan\mu_o/\tan\phi_o - 1}\mathcal{D} \tag{4.20}$$

yields the modified energy equation

$$\frac{\partial\theta}{\partial\xi} = \kappa\Delta e^{-\eta^2-\xi}e^{\theta}. \tag{4.21}$$

In these variables the characteristic equations (4.13) become

$$\frac{\partial\tilde{J}}{\partial\xi} = -\Delta e^{-\eta^2-\xi}e^{\theta}, \tag{4.22}$$

$$\frac{\partial\pi}{\partial\xi} = -\frac{B^-/B_T}{\tan\mu_o/\tan\phi_o + 1}\Delta e^{-\eta^2-\xi}e^{\theta}. \tag{4.23}$$

The problem at leading order reduces to the integration of the three ordinary differential equations (4.21)–(4.23) with boundary conditions $\tilde{J} = 0$ as $\xi \to \infty$ and $\theta = \tilde{J} = (B_T/B_p)\pi$ at $\xi = 0$ as follows from (4.17) and (4.18).

The reduced formulation indicates that the solution depends fundamentally on two parameters, namely, the reduced Damköhler number Δ of (4.20) and the parameter κ of (4.19), the latter measuring the competition between the cooling rate associated with the flow expansion induced by the chemical reaction

$$\frac{\gamma-1}{2\gamma}\frac{\partial}{\partial\xi}(J^+ + J^-) = -\frac{(\gamma-1)(\tan^2\mu_o+1)}{(\tan\mu_o/\tan\phi_o)^2-1}\mathcal{D}e^{-\eta^2-\xi}e^{\theta} \tag{4.24}$$

and the direct heat release rate of the chemical reaction $\mathcal{D}e^{-\eta^2-\xi}e^{\theta}$. The ratio of these two rates is the second term in the square brackets of (4.19). The direct heat release dominates when this ratio is smaller than unity, yielding positive values of κ, whereas the induced expansion prevails when it is larger than unity, yielding negative values of κ.

It is noteworthy that κ can be calculated in terms of the values of σ_o and M_o' of the approach shock unperturbed by the heat release, independently of the chemical reaction-rate parameters. Its iso-contours are plotted in figure 3. As can be seen in that figure, although depending on the incident-flow conditions this parameter may take either positive or negative values, corresponding to a temperature perturbation θ that either increases or decreases monotonically along the streamline (as indicated by (4.21)); it is positive in virtually all practical cases. The minimum value $\kappa = -1$, incidentally, is approached for weak shocks with $M_o' \sin\sigma_o = 1$.

Adding (4.22) times κ and (4.21) and integrating the resulting chemistry-free equation yields

$$\theta + \kappa\tilde{J} = (1+\kappa)\theta_s(\eta) \tag{4.25}$$

when the condition $\theta = \tilde{J}$ at $\xi = 0$ is used to evaluate the result. Using also the post-shock temperature θ_s to evaluate a first quadrature of (4.21) at $\xi = 0$ yields

$$\theta - \theta_s = \ln\left[1 - \kappa\Delta e^{-\eta^2} e^{\theta_s}(1 - e^{-\xi})\right]^{-1}. \tag{4.26}$$

Since $\tilde{J}$ must vanish as $\xi \to \infty$, the perturbed temperature distribution (4.26) must satisfy $\theta = (1+\kappa)\theta_s$ for $\xi \to \infty$, as follows from (4.25), thereby yielding the nonlinear algebraic equation,

$$\theta_s = \frac{1}{\kappa}\ln\left(\frac{1}{1 - \kappa\Delta e^{-\eta^2} e^{\theta_s}}\right), \tag{4.27}$$

which determines implicitly the post-shock temperature distribution $\theta_s(\eta)$ for given values of Δ and κ. The leading-order solution is completed by integrating a chemistry-free linear combination of (4.21) and (4.23) to give

$$\pi = \frac{B_p}{B_T}\theta_s - \frac{B^-/B_T}{\tan\mu_o/\tan\phi_o + 1}\frac{\theta - \theta_s}{\kappa}, \tag{4.28}$$

for the pressure perturbation resulting from the chemical reaction. Since B_p/B_T and B^-/B_T are always positive, the pressure perturbation given in (4.28) is largest at the shock, where $\pi_s = (B_p/B_T)\theta_s > 0$, and then decays monotonically with the streamwise distance ξ irrespective of the value of κ, in agreement with the negative sign preceding the reaction term in (4.23).

4.4. *Discussion of the results*

The leading-order solution for the temperature of the weakly reactive flow for $\gamma = 1.4$ is shown in figures 4–6. Figure 4 displays the variation with Δ of the peak post-shock temperature $\theta_s(0)$, reached at $\eta = 0$, for different values of κ, as obtained from evaluations of (4.27). It is seen that the resulting curves exhibit a turning point at

$$\Delta = \Delta_c = \left(\frac{1}{1+\kappa}\right)^{(1+\kappa)/\kappa}, \tag{4.29}$$

which can be obtained from straightforward differentiation of (4.27). Figure 4 indicates that the equation $\Delta = \Delta_c$ determines the critical condition for existence of a weakly reactive solution, in that no solution for $\theta_s(0)$ exists if $\Delta > \Delta_c$, while two values of

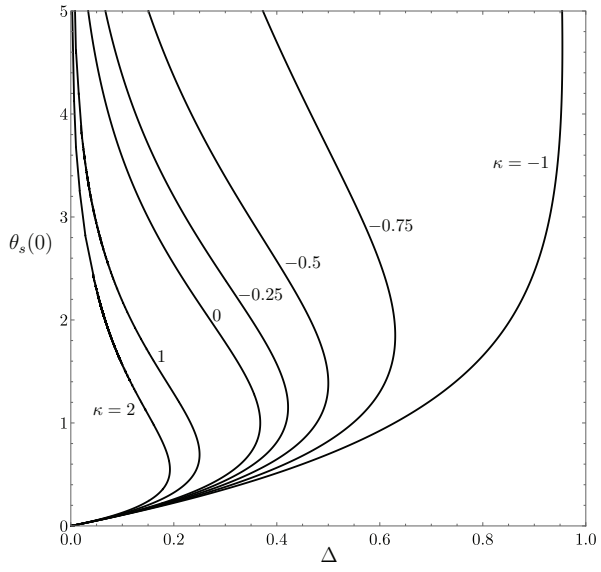

FIGURE 4. The variation of the rescaled temperature increment $\theta_s(0)$ with the Damköhler number Δ obtained from (4.27) for different values of the heating-rate parameter κ.

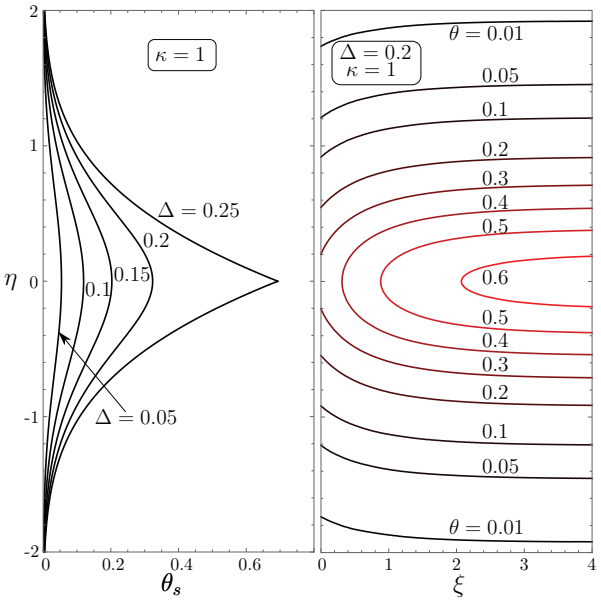

FIGURE 5. The temperature increase resulting from chemical reaction corresponding to a heating-rate parameter $\kappa = 1.0$ obtained from evaluations of (4.26) and (4.27), including post-shock temperature profiles $\theta_s(\eta)$ for different values of the Damköhler number Δ and isothermal curves for $\Delta = 0.2$.

$\theta_s(0)$ are found for $\Delta < \Delta_c$ when $\kappa > -1$, the upper value representing a non-physical, statically unstable condition. The limiting case $\kappa = -1$ of infinitesimally weak shocks, for which the curve in Figure 4 does not show a turning point but rather a vertical asymptote at $\Delta = 1$, is of limited interest in applications, because the associated temperature jump across the shock would be negligibly small.

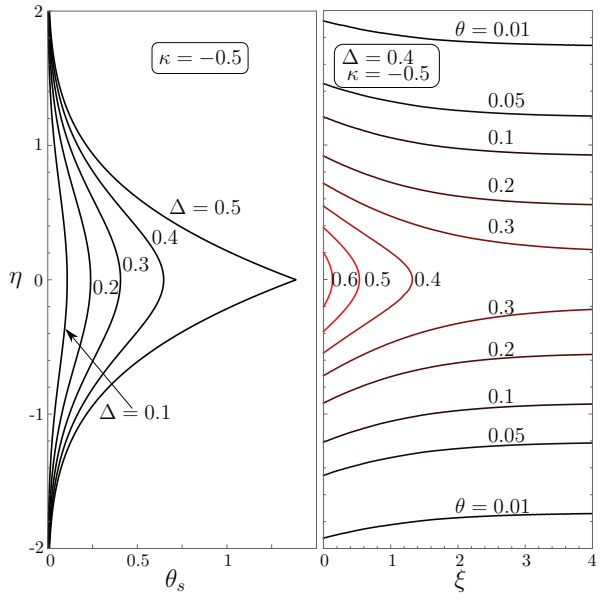

FIGURE 6. Same as figure 5 for $\kappa = -0.5$, with the isothermal curves plotted for $\Delta = 0.4$.

For values of $\Delta < \Delta_c(\kappa)$, therefore, the lower branch in the curve of figure 4 determines the peak shock temperature $\theta_s(0)$, while the associated temperature perturbation $\theta(\xi, \eta)$ is given by (4.26) once the shock distribution $\theta_s(\eta)$ is computed from (4.27). Sample results corresponding to $\kappa = 1$ are shown in figure 5. In particular, temperature distributions along the shock $\theta_s(\eta)$ are given for several values of Δ up to the ignition value Δ_c. The accompanying ignition-kernel field of perturbed temperature $\theta(\xi, \eta)$ is plotted for $\Delta = 0.2$. As expected, since the value of κ used in figure 5 is positive, the temperature perturbation θ is seen to increase downstream from the shock from the shock value θ_s, that being the situation encountered in most practical cases, as can be inferred from the evaluations of κ shown in figure 3. Negative values of κ in the range $-1 \leqslant \kappa < 0$, found in a thin parametric region adjacent to the infinitesimally weak boundary in figure 3, yield the opposite trend, that is, temperatures decreasing rather than increasing along the streamlines downstream from the shock, that being illustrated in figure 6 for $\kappa = -0.5$, which shows isocurves of $\theta(\xi, \eta)$ for $\Delta = 0.4$.

It is worth pointing out that the pressure increment induced by the heat release rate π can be readily evaluated in terms of the temperature perturbation using (4.28). Except for a positive scaling factor of order unity (B_p/B_T), the resulting pressure distribution along the shock $\pi_s(\eta) = (B_p/B_T)\theta_s(\eta)$ is identical to the temperature distribution $\theta_s(\eta)$ shown in figures 5 and 6. Unlike the temperature, however, the pressure is always a decreasing function of the distance from the shock ξ, as mentioned earlier.

For the diffusionless systems considered here it is remarkable that, in this configuration, ignition occurs as a fold bifurcation in the curve representing the peak value of the reactive perturbation (i.e., the value of θ_s or π_s at $\eta = 0$) as a function of the reduced Damköhler number Δ, with the critical conditions determined from a boundary-value problem of the Frank-Kamenetskii type in which pressure waves, rather than heat conduction, provide the basic energy transfer mechanism. Corrections to the leading-order results given here could be obtained by introducing expansions for the different flow variables in powers of $\beta^{-1/2}$. The first-order corrections would be associated with the

transverse derivatives neglected in (4.13), whereas computation of corrections of order β^{-1} and higher would require additional consideration of fuel consumption along with departures from the Frank-Kamenetskii linearization. Because of the presence of the turning point, in examining these higher-order terms one should pose the problem as that of determining the value of the parameter Δ that provides a given value of the temperature perturbation at the origin $\theta_s(0)$. Besides expansions for the different flow variables in powers of $\beta^{-1/2}$, an additional expansion $\Delta = \Delta_0 + \beta^{-1/2}\Delta_1 + \beta^{-1}\Delta_2 \cdots$ must then be introduced in the asymptotic solution for a fixed value of $\theta_s(0)$, with Δ_0 being the curve shown in figure 4, thereby enabling corrections to the bifurcation curve $\Delta - \theta_s(0)$ to be determined through the additional terms Δ_1, Δ_2, ... that would lead to improved predictions in the critical ignition Damköhler number.

5. Ignition near the hot boundary

In most practical supersonic-combustion devices, the air temperature at the entrance to the combustor is much larger than the temperature of the fuel. As a result, the peak temperature across the fuel-air mixing layer may still occur at the air boundary despite the effect of viscous dissipation. The oblique shock further increases this peak temperature, promoting the chemical reaction. Unlike the ignition scenario analyzed above, the amount of fuel available is limited when ignition occurs near the mixing-layer edge, so that fuel consumption needs to be accounted for when investigating the existence of weakly reactive solutions, as was done by Liñán & Crespo (1976) in their shock-free ignition analysis. It will be found that the resulting ignition kernel is nonslender, so that its description requires numerical integration of the complete ignition equations along the characteristic lines. It is worth pointing out that, although the analysis given here is for a one-step reaction with Arrhenius rate, mixing-layer ignition can be expected to occur always near the hot boundary whenever the controlling chemistry has a temperature dependence that is much stronger than the reactant-concentration dependence, as occurs for most fuels of practical interest, including hydrogen, for which the resulting homogeneous ignition times exhibit a moderately weak variation with the equivalence ratio but a much more pronounced dependence on the initial temperature (Sánchez & Williams 2014).

5.1. *Upstream flow profiles*

As seen in Appendix A, for a laminar mixing layer of thickness $\delta_m = 2[D_F x/U'_\infty]^{1/2}$, defined in terms of the fuel diffusivity D_F, with streamwise location $x \gg \delta_m$ and airstream velocity U'_∞, the profiles of fuel mass fraction Y, Mach number $\bar{M}' = M' - M'_\infty$, and temperature $\bar{T}' = (T' - T'_\infty)/T'_\infty$ admit near the air side the universal description

$$-\bar{M}' = -\frac{\bar{T}'}{\Gamma_T} = \frac{Y}{\Gamma_Y} = C\frac{\exp[-(z/\delta_m)^2]}{(z/\delta_m)}, \tag{5.1}$$

including identical exponential decay rates when all molecular diffusivities are taken to be equal (i.e., unity Prandtl and Lewis numbers). Here, the factors C, Γ_T, and Γ_Y are positive constants of order unity, whose specific values depend on the upstream mixing-layer evolution and the boundary conditions found on the fuel side.

The ignition kernel is defined in this case by the near-edge region where we find relative departures of the post-shock temperature from its boundary value T_∞ to be of order β^{-1}, now with $\beta = T_a/T_\infty$, since the maximum immediate post-shock temperature T_o now is T_∞. The kernel, then, occurs at the small values $\bar{M}' \sim \bar{T}' \sim Y \sim \beta^{-1}$. For definiteness,

we shall define the transverse location z_i of the ignition kernel from the equation

$$-\bar{M}' = \beta^{-1} = C\frac{\exp[-(z_i/\delta_m)^2]}{(z_i/\delta_m)}, \tag{5.2}$$

yielding an asymptotically large value $(z_i/\delta_m) \sim (\ln\beta)^{1/2}$. For the description of the ignition kernel, the origin of the nondimensional streamwise and cross-stream coordinates s and n will be placed at the shock-front location where $z = z_i$.

Expanding (5.1) about z_i reveals that the transverse dimension of the ignition region δ_i where we find relative variations of the different properties of order β^{-1} is of order $\delta_i/\delta_m \sim (z_i/\delta_m)^{-1} \sim (\ln\beta)^{-1/2} \ll 1$. For the analysis of ignition events near the hot boundary it is convenient to use this characteristic length δ_i to scale the problem, so that the resulting dimensionless coordinates s and n will differ from those appearing in the starting equations (3.1)–(3.4). Adopting the specific expression

$$\frac{\delta_i}{\delta_m} = \left(\frac{2z_i}{\delta_m}\right)^{-1}\frac{\sin\phi_\infty}{\sin\sigma_\infty} \tag{5.3}$$

for defining the characteristic length δ_i reduces the expansion of the upstream boundary distributions (5.1), up to terms of order $(\ln\beta)^{-1/2}$, to

$$-\beta\bar{M}' = -\beta\frac{\bar{T}'}{\Gamma_T} = \beta\frac{Y}{\Gamma_Y} = e^{-n}, \tag{5.4}$$

with n used to identify a given point along the shock front $s + n/\tan\phi_\infty = 0$.

5.2. *Problem formulation*

Introducing the rescaled variables

$$y = \beta\frac{Y}{\Gamma_Y}, \quad \Theta = \beta\frac{T - T_\infty}{T_\infty}, \quad \text{and} \quad \mathcal{J}^\pm = \beta\left(\frac{p - p_\infty}{p_\infty} \pm \frac{\gamma M_\infty^2}{\sqrt{M_\infty^2 - 1}}\frac{V}{U_\infty}\right), \tag{5.5}$$

of order unity in the ignition region, reduces the conservation equations, (3.6) and (3.8) with (3.4), to

$$\frac{\partial\mathcal{J}^\pm}{\partial s} \pm \tan\mu_\infty\frac{\partial\mathcal{J}^\pm}{\partial n} = \gamma(\tan^2\mu_\infty + 1)qDye^\Theta \tag{5.6}$$

$$\frac{\partial\Theta}{\partial s} - \frac{\gamma - 1}{2\gamma}\frac{\partial}{\partial s}(\mathcal{J}^+ + \mathcal{J}^-) = qDye^\Theta, \tag{5.7}$$

$$\frac{\partial y}{\partial s} = -Dye^\Theta, \tag{5.8}$$

where the relevant Damköhler number and heat-release parameters now are

$$D = \frac{B\beta e^{-\beta}}{U_\infty/\delta_i} \quad \text{and} \quad q = \frac{\Gamma_Y\tilde{q}}{c_pT_\infty}, \tag{5.9}$$

the former involving the characteristic residence time U_∞/δ_i in the ignition kernel, consistent with the scale δ_i selected for the coordinates s and n. Since the air stream is uniform, we must impose $\mathcal{J}^- = 0$ for the value of $\mathcal{J}^-$ approaching the ignition kernel

along each characteristic C^-. The additional conditions

$$y = e^{-n}, \tag{5.10}$$

$$\Theta = -\left(\Gamma_T + A_T - \frac{B_T}{B^-}A^-\right)e^{-n} + \frac{B_T}{B^-}\mathcal{J}^-, \tag{5.11}$$

$$\mathcal{J}^+ = -\left(A^+ - \frac{B^+}{B^-}A^-\right)e^{-n} + \frac{B^+}{B^-}\mathcal{J}^- \tag{5.12}$$

apply along the shock front $s = -n/\tan\phi_\infty$. Equation (5.10) states that the composition does not change across the shock, while (5.11) and (5.12) correspond to the linearized Rankine-Hugoniot conditions (3.15) and (3.16).

As before, it is convenient to formulate the problem by isolating the pressure and temperature perturbations introduced by the chemical reaction with use of the modified variables $\Theta_R = \Theta - \Theta_F$ and $\mathcal{J}_R^\pm = \mathcal{J}^\pm - \mathcal{J}_F^\pm$, where the subscripts F and R denote in each expression the chemically frozen solution and the reactive perturbation thereto, respectively. In the absence of chemical reaction $\mathcal{J}_F^- = 0$ everywhere. Using this result in evaluating the boundary condition (5.12) for $\mathcal{J}_F^+$ and integrating (5.6) along the C^+ characteristics gives

$$\mathcal{J}_F^+ = -\left(A^+ - \frac{B^+}{B^-}A^-\right)\exp\left(-\frac{n - s\tan\mu_\infty}{\tan\mu_\infty/\tan\phi_\infty + 1}\right). \tag{5.13}$$

This can be used, together with the condition $\mathcal{J}_F^- = 0$, to compute the pressure-gradient term in (5.7). Integrating the resulting equation with the boundary value of Θ_F at the shock evaluated from (5.11) with $\mathcal{J}^- = 0$ provides

$$\Theta_F = -E_P e^{-n}\left[\exp\left(\frac{s + n/\tan\phi_\infty}{1/\tan\phi_\infty + 1/\tan\mu_\infty}\right) - 1\right] - E_T e^{-n} \tag{5.14}$$

where

$$E_P = \frac{\gamma - 1}{2\gamma}\left(A^+ - \frac{B^+}{B^-}A^-\right) \quad \text{and} \quad E_T = \Gamma_T + A_T - \frac{B_T}{B^-}A^-. \tag{5.15}$$

The accompanying chemically frozen fuel mass fraction, determined by integration of $\partial y/\partial s = 0$ with boundary condition $y = e^{-n}$ at $s = -n/\tan\phi_\infty$, is simply given by $y_F = e^{-n}$. For the formulation below, which employes the reactive perturbations Θ_R and $\mathcal{J}_R^\pm$, we choose not to express y as the sum of y_F and the perturbation associated with the chemical reaction, because for that variable the decomposition does not result in any significant simplification.

The reactive perturbations are determined by integrating

$$\frac{\partial \mathcal{J}_R^\pm}{\partial s} \pm \tan\mu_\infty \frac{\partial \mathcal{J}_R^\pm}{\partial n} = \gamma(\tan^2\mu_\infty + 1)qDye^{\Theta_F + \Theta_R} \tag{5.16}$$

$$\frac{\partial \Theta_R}{\partial s} - \frac{\gamma - 1}{2\gamma}\frac{\partial}{\partial s}(\mathcal{J}_R^+ + \mathcal{J}_R^-) = qDye^{\Theta_F + \Theta_R} \tag{5.17}$$

$$\frac{\partial y}{\partial s} = -Dye^{\Theta_F + \Theta_R}, \tag{5.18}$$

with boundary conditions

$$y = e^{-n} \quad \text{and} \quad \frac{\Theta_R}{B_T} = \frac{\mathcal{J}_R^-}{B^-} = \frac{\mathcal{J}_R^+}{B^+} \tag{5.19}$$

at the shock front $s = -n/\tan\phi_\infty$ and a vanishing value

$$\mathcal{J}_R^- = 0 \tag{5.20}$$

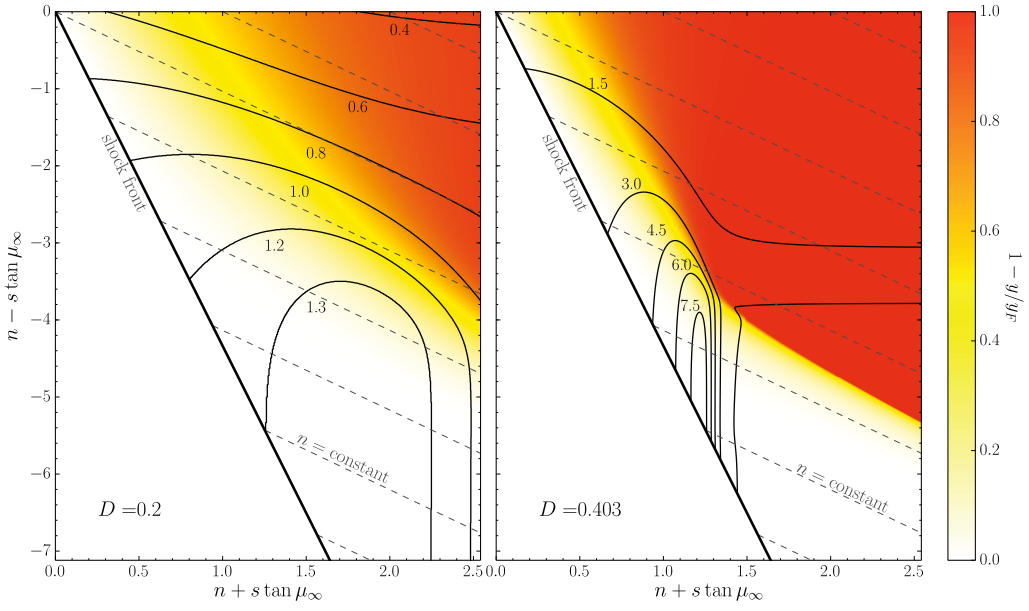

FIGURE 7. The ignition kernel obtained by numerical integration of (5.16)–(5.18) for $M'_\infty = 5$, $\sigma_\infty = 20^\circ$, $\gamma = 1.4$, $\Gamma_T = 1$, and $q = 2$ for $D = 0.2$ and for $D = 0.403$. The shaded contours represent the fraction of heat released $1 - y/y_F$ while the solid curves are isolines of pressure increment due to chemical reaction $\pi = (\mathcal{J}_R^+ + \mathcal{J}_R^-)/2$.

on the air boundary (i.e., for $n \to \infty$ and $s > -n/\tan\phi_\infty$).

Straightforward evaluations of the different Rankine-Hugoniot functions for given values of M'_∞, σ_∞, and γ provide the constants A_T, B_T, A^+, A^-, B^+, and B^- as well as the values of the flow deflection ν_∞ and the post-shock Mach number M_∞ needed to determine the angles $\mu_\infty = \sin^{-1}(M_\infty^{-1})$ and $\phi_\infty = \sigma_\infty - \nu_\infty$. The additional parameters involved in the problem are related to the shape of the temperature profile upstream from the shock, which enters in the formulation through the parameter Γ_T appearing in (5.15), and to the chemical reaction, which enters through the reduced chemical heat release q and the Damköhler number D.

5.3. *Discussion of results*

Equations (5.16)– (5.18) subject to the boundary conditions given in (5.19) and (5.20) were solved numerically by integrating along the three characteristics with a first-order explicit method, giving the results shown below in figures 7–9. These sample integrations correspond to $\Gamma_T = 1$ with $M'_\infty = 5$, $\sigma_\infty = 20^\circ$, and $\gamma = 1.4$, yielding $A_T = 0.168$, $B_T = 2.31$, $A^+ = 0.191$, $A^- = 0.651$, $B^+ = -0.240$, $B^- = 11.8$, $\mu_\infty = 14.7^\circ$, and $\phi_\infty = 9.33^\circ$. Different values of q and D were considered to investigate the dependence of the solution on the reaction exothermicity and on the reaction rate, as discussed below.

5.3.1. *The structure of the ignition kernel*

Figure 7 shows ignition kernels for $q = 2$ and two different values of D. The solution is represented with use made of $n - s\tan\mu_\infty$ and $n + s\tan\mu_\infty$ in the abscissa and ordinate axes, so that the C^- and C^+ characteristics are vertical and horizontal lines in the plots, respectively, while the streamlines $n =$ constant appear as oblique lines with negative slope. The region where chemical reaction occurs is revealed by using shaded contours for the fraction of heat released $1 - y/y_F$, where $y_F = e^{-n}$ is the chemically frozen

fuel mass fraction. The structure of the ignition kernel is visualized with use made of the pressure perturbation produced by the chemical reaction $\pi = (\mathcal{J}_R^+ + \mathcal{J}_R^-)/2$, which progressively grows in the ignition kernel with increasing values of the Damköhler number until ignition conditions are reached for a critical value of D of order unity. The lower Damköhler number $D = 0.2$ selected in figure 7 is illustrative of conditions far from ignition, while $D = 0.403$ corresponds to the largest Damköhler number for which a solution could be found in this case, as explained below.

The integration begins on the air side of the mixing layer, where the reactive perturbations are negligibly small as a result of the exponentially small fuel mass fraction found there. With negligible pressure perturbations, each fluid particle evolves independently in the quasi-isobaric background flow, burning downstream from the shock at a fixed finite distance that is inversely proportional to the Damköhler number, as can be seen by integrating (5.18) with $\Theta_F + \Theta_R = 0$ to give $y = e^{-n} \exp[-D(s + n/\tan\phi_\infty)]$, where $s + n/\tan\phi_\infty$ is the streamwise distance from the shock. This simple solution with finite induction length and exponentially small perturbations begins to evolve on approaching values of n of order unity, where the existing richer mixtures allow for more vigorous chemical reaction, whereas the lower unperturbed post-shock temperatures Θ_F tend to freeze the reaction rate. As in the case of ignition in the interior of the mixing layer analyzed earlier, the dynamics is further complicated by the existence of pressure waves induced by the chemical reaction, including expansion waves along the C^+ characteristics and compression waves along the C^- characteristics. The latter are seen to reach the shock, strengthening it and increasing the reaction rate immediately behind through the associated temperature increase.

The interplay between all of these competing effects results in the ignition-kernel structures displayed in figure 7. The integrations reveal that the decreasing value of the background temperature Θ_F eventually becomes dominant for sufficiently large negative values of $-n \gg 1$, preventing the chemical reaction from occuring in the vicinity of the shock. As $-n$ increases, the background post-shock temperature decreases rapidly according to $\Theta_F = -E_T e^{-n}$, resulting in induction lengths that become increasingly large. The associated reaction layer separating the fresh mixture from the hot products turns away from the shock, evolving to approach asymptotically the streamline slope as the induction length becomes exponentially large, as seen clearly on the right-hand-side plot in figure 7.

5.3.2. *Ignition as a fold bifurcation*

For the value of the heat release $q = 2$ selected in the integrations of figure 7 the numerical integrations failed to converge for values of $D > 0.403$, the right-hand-side in the figure representing the critical case $D = 0.403$. Additional computations using refined grids and implicit rather than explicit integration schemes did not modify this critical maximum value. The critical solution displayed on the right-hand side of figure 7, involving an ignition kernel with finite induced pressure, exhibits a rather sharp transition from a solution with constant induction length to a solution with an exponentially increasing induction length.

The results indicate that the mechanism leading to ignition is similar to that encountered when ignition occurs at a local temperature maximum inside the mixing layer, in that in both cases ignition occurs as a fold bifurcation in the curve representing the peak perturbation induced by the chemical reaction in terms of the relevant Damköhler number. In the present analysis, it is convenient to use the induced pressure perturbation π as a representation of the extent of the chemical reaction, since the increase of this quantity is a suitable measure of the pressure-reaction interactions leading to ignition.

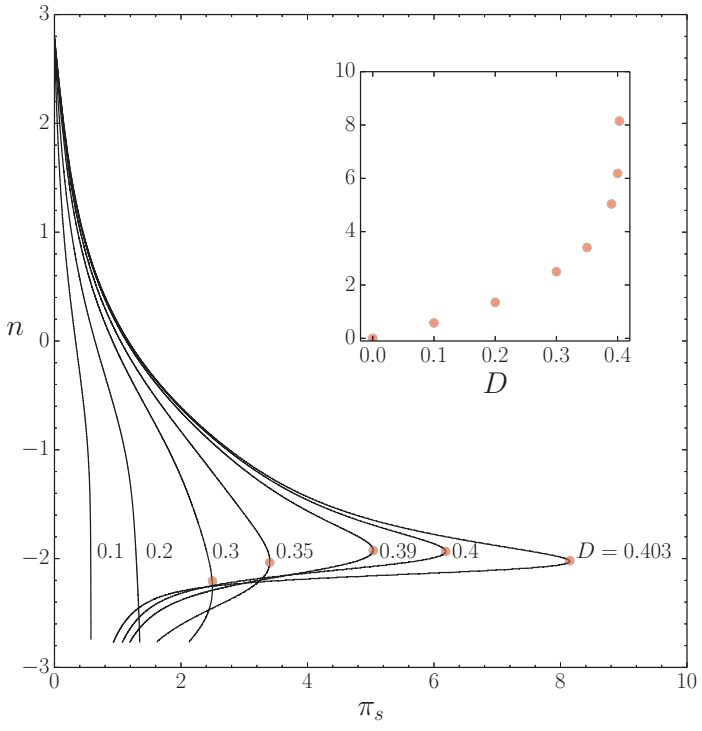

FIGURE 8. The pressure increase resulting from chemical reaction along the shock obtained for different values of D with $M'_\infty = 5$, $\sigma_\infty = 20^\circ$, $\gamma = 1.4$, $\Gamma_T = 1$, and $q = 2$; the inset represents the evolution of the peak value of π_s with D.

As in the case of ignition at a temperature maximum, the peak value of π is seen to occur always adjacent to the shock. Therefore, to illustrate the bifurcation character of the ignition process, profiles of perturbed pressure along the shock π_s are represented in figure 8 for different values of the Damköhler number D, including the values $D = 0.2$ and $D = 0.403$ considered in figure 7. The resulting curves are to be compared with those given in figures 5 and 6 for θ_s, the latter proportional to π_s according to (4.28). In both cases, the pressure perturbation develops a sharp peak as D approaches the critical value. The rapid variation of the peak pressure near the critical conditions is shown in an inset of figure 8, which constitutes the appropriate bifurcation curve in this case, fundamentally equivalent to the curves shown in figure 4 for ignition at a local temperature maximum. While the previous analytical results of § 4 enabled the description of the whole bifurcation curve to be derived, only the lower branch of the bifurcation curve up to the turning point is described in the inset of figure 8, the upper branch corresponding to unstable solutions that are not accessible in the numerical integrations.

The critical value of D at bifurcation depends strongly on the parameter q, a nondimensional measure of the heat released per unit mass of fuel burnt. As the value of q decreases the effect of fuel consumption becomes more significant, with the consequence that the development of ignition requires a larger Damköhler number when all other flow parameters are kept unchanged. This is illustrated in figure 9, where it can be seen that the exponential dependences present in the problem translate into a strong depen-

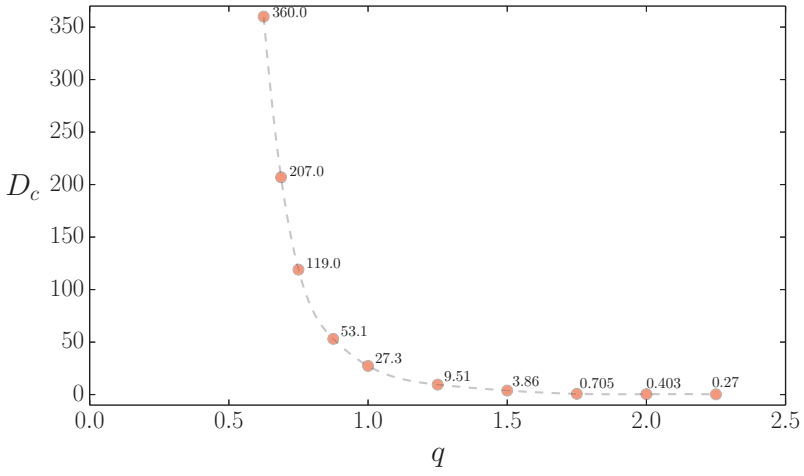

FIGURE 9. The variation with q of the critical Damköhler number at ignition as obtained from numerical integrations for $M'_\infty = 5$, $\sigma_\infty = 20^\circ$, $\gamma = 1.4$, and $\Gamma_T = 1$.

dence of the ignition Damköhler number on q. In corresponding problems for which heat conduction rather than acoustic-wave propagation is responsible for transmitting the temperature field generated by the chemical heat release at the edge of the mixing layer, as in Liñán & Crespo (1976), there is a critical value of q below which the fold bifurcation disappears and is replaced by a continuous transition to a thin diffusion flame involving a lean deflagration propagating across the mixing layer from the hot boundary. The physical mechanism for this continuous development is not present in the inviscid problem addressed here. The fold bifurcation therefore persists, the critical Damköhler number for ignition growing to extremely large values as q decreases, which may be inferred from figure 9.

6. Post-ignition scenarios

The local ignition analyses described in § 4 and § 5, which are based on investigations of small departures from the chemically frozen post-shock state, identified the critical conditions for existence of a weakly reactive solution in the vicinity of the most reactive point. Because of the strong temperature dependence of the chemical reaction rate, the size of the ignition kernel, defined as the streamwise length required for the post-shock expansion resulting from the front curvature to freeze the chemical reaction, is found to be a small fraction of the mixing-layer thickness δ_m. The ratio of the associated residence time (comparable to the acoustic time in the limit considered here), to the relevant chemical time evaluated with the local peak temperature, defines the relevant Damköhler number of the flow. Ignition is found to be associated with a critical Damköhler number above which no solution to the Frank-Kamenetskii ignition problem is found.

For subcritical values of the Damköhler number the flow expansion freezes the chemical reaction at the edge of the ignition kernel. Since the total amount of fuel consumed is negligibly small, the associated reactive perturbations can be neglected in the first approximation when describing the flow outside. The nonreacting inviscid mixing layer continues to evolve in a nonslender post-shock region of characteristic size δ_m, where we find relative pressure variations of order unity. At downstream distances large compared with δ_m the inviscid evolution of the mixing layer ceases as the pressure settles

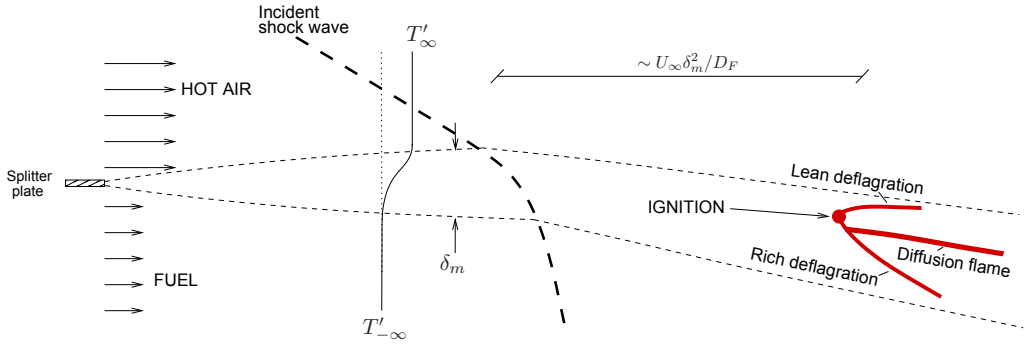

(a) Downstream ignition detached from shock

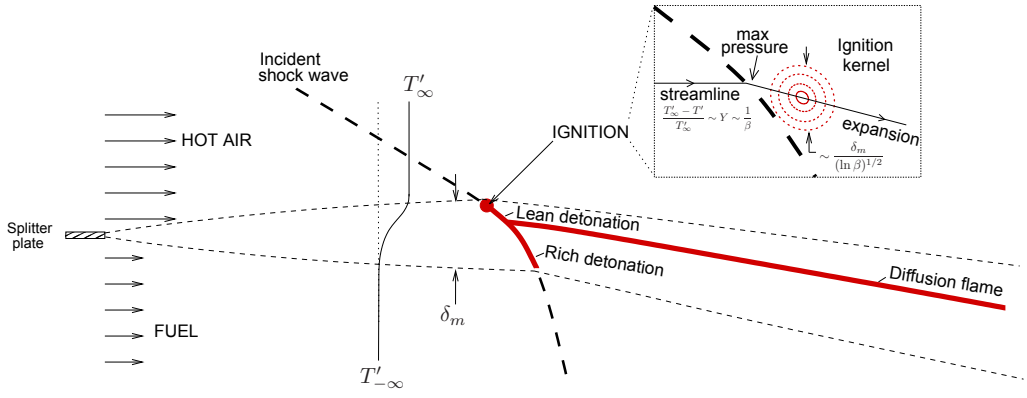

(b) Shock−induced ignition near the hot boundary

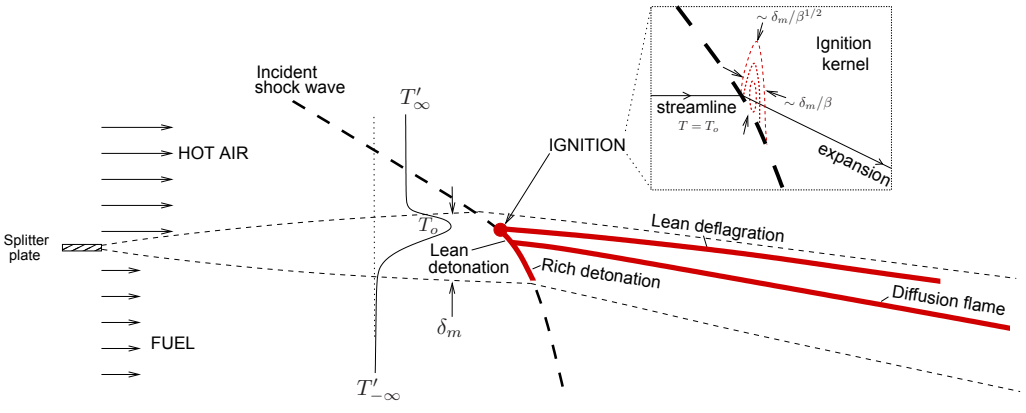

(c) Shock−induced ignition at a local temperature maximum

FIGURE 10. Schematic view of different post-shock configurations corresponding to (a) subcritical values of the Damköhler number, (b) shock-induced ignition near the airside boundary, and (c) shock-induced ignition in the interior of the mixing layer above the stoichiometric point; the insets in (b) and (c) represent the ignition kernels for the weakly reactive solutions described in § 5 and in § 4, respectively.

to a uniform value, intermediate between p'_∞ and p_∞. The inviscid acoustic interactions leave the mixing layer deflected at an angle that depends on the Mach numbers M'_∞ and $M'_{-\infty}$ of the incoming streams and that can be calculated from the angle of the slip stream in the classical wave-interaction description (Landau & Lifshitz 1987). This downstream mixing layer will have modified transverse distributions of temperature,

Mach number, and species mass fractions as a consequence of the acoustic interactions that it has experienced. The subsequent evolution of the mixing layer that emerges from the acoustic region occurs over long distances that are of order $U_\infty \delta_m^2/D_F \gg \delta_m$, associated with residence times of the order of the diffusion time across the mixing layer δ_m^2/D_F. The resulting slender isobaric flow can be described in the boundary-layer approximation, accounting for the effect of viscous dissipation. An analysis analogous to that of Liñán & Crespo (1976) would be necessary for assessing the occurrence of ignition in this downstream region in terms of an alternative ignition Damköhler number involving the ratio of the residence time δ_m^2/D_F to the characteristic chemical time based on the post-shock conditions downstream from the acoustic region. The resulting flow is schematically represented in figure 10(a).

For supercritical values of the Damköhler number there must exist cases with very large activation energies and small heat-release parameters, corresponding to very large Damköhler numbers, in which the total amount of post-ignition heat release remains everywhere small compared with the local thermal enthalpy, allowing the heat release to evolve as a perturbation in a flow that is supersonic everywhere. This heat release, which would remain inviscid if the characteristic heat-release time remains small compared with the cross-stream diffusion time, could not result in an evolution to a weak detonation because the near-Rayleigh-line flow would encounter the strong-detonation branch first. The weak-heat-release perturbation to the nonreacting flow field thus would result in strongly overdriven detonations, varying in the transverse direction across the deflected mixing layer. Since the wave-interaction processes that are responsible for the approach to Chapman-Jouguet conditions are likely to be insufficient, the oblique detonations would remain strong in most cases, and with the increasing heat release associated with increasing fuel concentration this would result in the near-shock region developing a significantly perturbing vigorous chemical reaction in a short induction region of thickness much smaller than the size of the ignition kernel. The tendency towards onset of the well-known cellular instability of detonations with the decreasing overdrive caused by the increased heat release may well give rise to an instability that drives the lead shock away from it smooth trajectory of evolution, generating cells. The flow field nevertheless would remain supersonic everywhere if the detonation were sufficiently oblique and the Mach-number change across the mixing layer were small enough, but in many realistic situations the flow in the (x, z) fixed frame will become subsonic downstream from the lead shock of the detonation. While this introduces local elliptic acoustic interactions that will affect the strength of the detonation and therefore its manner of evolution across the mixing layer, it cannot modify the approaching mixing layer, which is supersonic throughout.

Computation of the propagation of the detonation across the mixing layer and the evolution of its strength is a very challenging problem in gas dynamics with finite-rate heat release. The description is simplified when an infinitely fast reaction model is adopted for the ignited section of the shock front (i.e., below the ignition point), with the resulting detonation appearing in the first approximation as an infinitesimally thin front separating the unperturbed cold flow from the equilibrium products. In this approximation, the computation of the flow at distances of order δ_m requires integration of the Euler equations subject to modified Rankine-Hugoniot conditions including a jump in stagnation enthalpy that depends on the transverse location through the associated upstream distribution of reactants. If ignition occurs at the hot boundary, as described in § 5, then the modified jump conditions would apply all across the mixing layer, and the associated post-shock flow would be everywhere in equilibrium, resulting in the flow configuration sketched in figure 10(b). By way of contrast, if ignition occurs at an intermediate location,

the case considered in § 4 represented schematically in figure 10(c), then a nonreacting shock would be found above the ignition point and a detonation front below, with the downstream streamline departing from the ignition point correspondingly separating a chemically frozen region from a region in chemical equilibrium, across which a deflagration aligned with the flow eventually should develop far downstream, where molecular transport becomes relevant. If the flow downstream from the shock remains supersonic, then the conservation equations can be formulated in characteristic form, resulting in a problem, similar to that described in § 2 for the shock-wave/mixing-layer interaction, that would determine the shock and detonation front shapes. Correspondingly, an approximation equivalent to that of Moeckel (1952) could be useful in that case to derive an explicit expression for the distribution of the incident angle $\sigma(z)$.

The shape of the detonation depends on the distribution of reactants, temperature, and Mach number across the mixing layer, as well as on the post-shock and post-detonation thermodynamic states that vary with these properties and that affect the shape through inviscid interactions carried (if the flow remains supersonic) by the characteristics that reach the front. The heat release is maximum at the stoichiometric point and then decreases towards the fuel side as the mixture becomes richer. For ignition near the air-side boundary, as occurs when the variations of $T'(z)$ and $M'(z)$ are not too pronounced, one possible result that may be expected to arise when the effect of heat release is dominant in determining the shape of the detonative front is that the detonative front may evolve from concave to convex, including an inflection point near the stoichiometric point. The detonation remains concave when the upstream velocity across the mixing layer decreases sufficiently rapidly towards the fuel side, giving a front shape similar to that of the non-reacting situation, that being the case represented in figure 10(b). Since the streamline originating at the stoichiometric point separates a region without fuel from a region without oxygen, a trailing diffusion flame develops through molecular transport processes, extending far downstream, burning the excess oxygen found above the stoichiometric point (i.e, behind the fuel-lean section of the detonation) with the excess fuel found below (i.e, behind the fuel-rich section of the detonation). Overall, this constitutes a tribrachial structure, including a detonative front with lean and rich branches on both sides of the stoichiometric point, which serves as the origin for a trailing diffusion flame that extends over streamwise distances of the order of δ_m times the local Reynolds number. Illustrated in figure 10(b), this can be compared with the structure identified by Liñán & Crespo (1976) in their shock-free ignition analysis, with the lean and rich detonative fronts replacing in our case the deflagrations of their analysis.

The resulting flow structure is more complicated when ignition occurs in the middle of the mixing layer. The schematic view of figure 10(c) corresponds to this situation, with the ignition point separating the nonreacting shock found above from a detonation below. If the ignition point lies above the stoichiometric point, then the downstream flow evolution at distances of order $U_\infty \delta_m^2 / D_F \gg \delta_m$ includes a lean deflagration departing from the ignition point and a diffusion flame departing from the stoichiometric point, that being the case illustrated in figure 10(c). The downstream flow is different when the ignition point lies below the stoichiometric point. The rich deflagration that originates at the ignition point would propagate upwards as it develops, crossing the stoichiometric line, where it becomes lean. The diffusion flame develops only downstream from this crossing point, i.e., the flow along the stoichiometric streamline downstream from the shock remains chemically frozen until it is ignited by the deflagration crossing from below. Additional complicating effects may further modify the flow depicted in figure 10(c). For example, detonations may possibly develop on both sides of the ignition point for a sufficiently strong ignition kernel, and possibilities of detonation failure as weak mix-

tures are approached in the wings raise further uncertainties. All of these considerations illustrate the wealth of novel phenomena that may arise from shock-wave/mixing-layer interactions in the presence of chemical reactions.

The above descriptions assume that the ignition kernel serves to anchor the detonation. If the mixture were sufficiently reactive for the propagation velocity of the strong detonation to be sufficiently high and the incoming stream were sufficiently slow, then the resulting detonation could propagate upstream along the mixing layer. For smaller values of x the detonation front would then encounter increasing transverse gradients, resulting in a decreasing propagation velocity, as discussed by Calhoon & Sinha (2005). Eventually, a liftoff location woud be reached at which the detonation is stabilized. Although studies of detonations propagating in transverse gradients have been attempted recently Kessler et al. (2012), much further work is warranted to assess the relevance of this phenomenon in connection with SCRAMJET combustion applications.

7. Concluding remarks

The ignition analyses that have been developed here help to clarify the manner in which shock waves may promote ignition in supersonic mixing layers to lead to establishment of diffusion flames in supersonic flows. Two different conditions have been identified, one in which ignition first occurs in the interior of the mixing layer, in the vicinity of the point at which the post-shock gas temperature is a maximum, and the other in which the ignition develops at the hot-stream edge of the mixing layer. While the analyses are different for these two conditions, the first being analytical but the second necessitating both numerics and taking reactant consumption into account, they both lead to fold-bifurcation descriptions of ignition in a Frank-Kamenetskii approach. A novel aspect is that, for these shock-induced ignition problems, the cooling processes that compete with the chemical heat release involve inviscid gasdynamic acoustic-wave propagation instead of the familiar diffusive heat conduction. The description, however, applies only to one-step Arrhenius heat-release chemistry with a large activation energy. Further research is warranted for investigating the extent to which this description may apply to the heat-release chemistry of real SCRAMJET fuels, such as hydrogen.

It is worth mentioning that the condition for the validity of the ignition analyses developed here is that the flow is supersonic across the ignition kernel and above (in the post-shock region that extends towards the high-speed air stream), regardless of whether the flow eventually becomes subsonic on the fuel side outside the ignition kernel. For example, the local descriptions of the ignition kernels and the resulting critical ignition conditions apply also to configurations involving transonic mixing layers with subsonic fuel streams, provided that the ignition kernel is located sufficiently close to the air side for the post-shock flow to remain locally supersonic.

A further aspect worthy of emphasis is the fact that the analysis has been developed here only for laminar mixing layers, while the supersonic flow is turbulent in the vast majority of situations of interest. The competing mechanisms identified in connection with the laminar case can be anticipated to play also a fundamental role in turbulent environments. Since in turbulent mixing-layer flows the fluctuations of temperature and velocity are relatively small compared with the local mean values, it is the profiles of mean temperature and velocity found upstream from the shock-wave impingement point that determine in the first approximation the mean curvature of the shock across the mixing layer as well as the resulting transverse profile of mean post-shock temperature. Just as in the laminar case considered here, because of the high temperature sensitivity of the reaction rate ignition in turbulent flows tends to occur around the point of peak

temperature, and the dominant cooling mechanism competing with the chemical heat release to determine the size of the ignition kernel is the postshock expansion resulting from the mean shock-front curvature. This leads to negative streamwise temperature gradients comparable to the mean transverse gradients, thereby much larger than those associated with the streamwise turbulent heat flux. These considerations indicate that in the presence of turbulence the location and size of the ignition kernel could be determined to a good approximation from the computation of the steady inviscid interaction of the incident shock with the pre-shock transverse profiles of mean temperature and velocity, the latter computed by merely replacing the laminar diffusivities of the mixing layer by turbulent diffusivities.

Despite these similarities between the laminar and turbulent cases, the ignition dynamics in turbulent flows can be expected to be very different owing to the role of turbulent temperature fluctuations (Libby & Williams 1980). In particular, although the size and location of the ignition kernel are not affected strongly by turbulence, the resulting critical ignition conditions would differ significantly from those evaluated by simply applying the formulae developed here to the mean profiles of turbulent flow, especially when ignition occurs near the air side, where the ignition dynamics is more sensitive to intermittent fluctuations. Because of the strong temperature dependence present in the problem, ignition would be affected mainly by the most energetic eddies associated with the integral scales, which have the largest fluctuations of temperature, and also the largest fluctuations of velocity, the latter leading to shock wrinkling causing additional temperature fluctuations comparable in magnitude to those found in the mixing layer upstream from the shock. The role of the smaller eddies all the way down to the Kolmogorov scale is expected to be secondary, so that the influence of turbulence remains inviscid and could be addressed in the framework of the unsteady Euler equations. Earlier work on interactions of turbulence with shock waves and detonations becomes relevant in that respect (e.g., see Huete et al. (2013, 2014) and references therein). Large-eddy simulation of supersonic turbulent ignition problems (O'Brien et al. 2014) should account for the interactions identified herein in guiding developments of appropriate local subgrid models for shock-induced ignition. A great deal of additional research therefore remains to be done in this general area.

This work was supported by the US AFOSR Grant # FA9550-12-1-0138.

Appendix A.

Simplified expressions for the shape of the different profiles at the edge of the mixing layer can be obtained by considering the simplified boundary-layer form of the conservation equations near the air boundary. For instance, the transport equation for the fuel takes the form

$$U'_\infty \frac{\partial Y}{\partial x} + V'_\infty \frac{\partial Y}{\partial z} = D_F \frac{\partial^2 Y}{\partial z^2}, \tag{A 1}$$

with U'_∞ representing the free airstream velocity, $V'_\infty < 0$ the entrainment velocity, and D_F the molecular diffusivity of the fuel. At a given downstream location x, the decay of the fuel mass fraction as z increases can be expressed as

$$Y \propto \mathrm{erfc}\left\{[z - z_Y - \int_0^x (V'_\infty/U'_\infty)\mathrm{d}x]/\delta_m\right\}, \tag{A 2}$$

an exact solution of (A 1) involving the transverse translation z_Y and the local mixing-layer thickness $\delta_m = 2[D_F x/U'_\infty]^{1/2}$, with erfc representing the complementary error

function. If needed for increased accuracy, this description can be corrected by incorporation of a virtual origin in the streamwise coordinate x.

For $z \gg \delta_m$ the error-function expression (A 2) simplifies to

$$Y \propto \exp[-(z/\delta_m)^2]/(z/\delta_m). \tag{A 3}$$

If, in addition, all molecular diffusivities are taken to be equal by assuming unity Prandtl and Lewis numbers in writing the boundary-layer form of the energy and momentum equations near the mixing-layer edge, then similar expressions of the form $(T' - T'_\infty)/T'_\infty \propto \exp[-(z/\delta_m)^2]/(z/\delta_m)$ and $(U' - U'_\infty)/U'_\infty \propto \exp[-(z/\delta_m)^2]/(z/\delta_m)$ are obtained for the temperature and streamwise-velocity departures from the airside values. These can be used to finally express the near-edge solution in the form

$$-\bar{M}' = -\frac{\bar{T}'}{\Gamma_T} = \frac{Y}{\Gamma_Y} = C\frac{\exp[-(z/\delta_m)^2]}{(z/\delta_m)}, \tag{A 4}$$

where the factors C, Γ_T, and Γ_Y are positive constants of order unity, whose specific values, which vary with the temperature and velocity of the fuel stream, depend on the evolution of the flow upstream from the location x considered.

REFERENCES

Buttsworth, D. R. 1996 Interaction of oblique shock waves and planar mixing regions. *J. Fluid Mech.*, **306**, 43–57.

Brummund, U. & Nuding, J. R. 1997 Interaction of a compressible shear layer with shock waves - an experimental study. *AIAA Paper*, 0392.

Calhoon, W. H. & Sinha, N. 2005 Detonation wave propagation in concentration gradients. *AIAA Paper*, 1167.

Dolvin, D. 2008 Hypersonic International Flight Research and Experimentation (HiFiRE). *AIAA Paper*, 2581.

Frank-Kamenetskii, D. A. 1969 *Diffusion and Heat Transfer in Chemical Kinetics*, Second ed., Plenum Press, New York, NY.

Génin, F. & Menon, S. 2010 Studies of shock/turbulent shear layer interaction using large-eddy simulation. *Comput. Fluids* **39** 800–819.

Grosch, C. E. & Jackson, T. L. 1991 Ignition and structure of a laminar diffusion flame in a compressible mixing layer with finite rate chemistry. *Phys. Fluids A* **3**, 3087–3097.

Gutmark, E. J., Schadow, K. C., & Yu, K. H. 1995 Mixing enhancement in supersonic free shear flows. *Ann. Rev. Fluid Mech.*, **27**, 375–417.

Hayes, W. D. & Probstein, R. F. 2004 *Hypersonic Inviscid Flow*, Second ed., Dover, Mineola, NY, pp. 480–484.

Huete, C., Sánchez, A. L., & Williams, F. A. 2013 Theory of interactions of thin strong detonations with turbulent gases. *Phys. Fluids*, **25**, 076105.

Huete, C., Sánchez, A. L., & Williams, F. A. 2014 Linear theory for the interaction of small-scale turbulence with overdriven detonations. *Phys. Fluids*, **26**, 116101.

Huete, C., Urzay, J., Sánchez, A. L., & Williams, F. A. 2015 Weak-shock interactions with transonic laminar mixing layers of fuels for high-speed propulsion. *AIAA J.* to appear.

Jackson, T. L. & Hussaini, M. Y. 1988 An asymptotic analysis of supersonic reacting mixing layers. *Combust. Sci. Technol.* **57** 129–140.

Kessler, D. A., Gamezo, V. N., and Oran, E. S. 2012 Gas-phase detonation propagation in mixture composition gradients. *Phil. Trans. R. Soc. A* **370**, 567–596.

Landau, L. D. & Lifshitz, E. M. 1987 *Fluid Mechanics*, Second ed., Pergamon Press, Oxford, England, pp. 422–423.

Laurence, S. J., Karl, S., Schramm, J., Martínez, J. & Hannemann, K. 2013 Transient fluid-combustion phenomena in a model scramjet. *J. Fluid Mech.* **722**, 85–120.

Libby, P. A. & Williams, F. A. 1980 *Turbulent Reacting Flows*, Springer-Verlag, Berlin, Germany, pp. 32–33.

Lighthill, M. J. 1950 Reflection at a laminar boundary layer of a weak steady disturbance to a supersonic stream, neglecting viscosity and heat conduction. *Quarter. J. Mech. Appl. Math.*, **3**, 303–325.

Lighthill, M. J. 1953 On boundary layers and upstream influence. II. Supersonic flows without separation. *Proc. Royal Soc. London A.*, **213**, 478–507.

Liñán, A. & Crespo, A. 1976 An asymptotic analysis of unsteady diffusion flames for large activation energies. *Combust. Sci. Technol.* **14** 95–117.

Lu, P. J. & Wu, K. C. 1991 On the shock enhancement of confined supersonic mixing flows. *Phys. Fluids A*, **3**, 3046–3062.

Marble, F. E., Hendricks, G. J. & Zukoski, E.E. 1987 Progress toward shock enhancement of supersonic combustion processes. *AIAA Paper*, 1880.

Marble, F. E. 1994 Gasdynamic enhancement of nonpremixed combustion. *Proc. Combust. Inst.*, **25**, 1–12.

Menon, S. 1989 Shock-wave-induced mixing enhancement in scramjet combustors. *AIAA Paper*, 0104.

Moeckel, W. E. 1952 Interaction of oblique shock waves with regions of variable pressure, entropy, and energy. *NACA Tech. Note* 2725.

Nuding, J. R. 1996 Interaction of compressible shear layers with shock waves: an experimental study, part I. *AIAA Paper*, 4515.

O'Brien, J., Urzay, J., Ihme, M., Moin, P. & Saghafian, A. 2014. Subgrid-scale backscatter in reacting and inert supersonic hydrogen-air turbulent mixing layers. *J. Fluid Mech.* **743**, 554–584.

Riley, N. 1960 Interaction of a shock wave with a mixing region, *J. Fluid Mech.*, **7**, 321–339.

Sánchez, A. L. & Williams, F. A. 2014 Recent advances in understanding of flammability characteristics of hydrogen. *Prog. Energy Combust. Sci.*, **41**,1–55.

Vázquez-Espí, C. & Liñán, A. 2001 Fast, non-diffusive ignition of a gaseous reacting mixture subject to a point energy source. *Combust. Theor. Model.* **5**, 485–498.

Waidmann, W., Alff, F., Brummund, U., Böhm, M., Clauss, W. & Oschwald M. 1994 Experimental investigation of the combustion process in a supersonic combustion ramjet (SCRAMJET) In: *DGLR Jahrestagung* pp. 629–638, Erlangen.

Whitham, G. B. 1958 On the propagation of shock waves through regions of non-uniform area or flow. *J. Fluid Mech.* **4**, 337–360.

Williams, F. A. 1985 *Combustion Theory*, Second ed., Benjamin Cummings, Menlo Park, CA, pp. 576–581.

Zhang, Y., Wang, B., Zhang, H., & Xue, S. 2015 Mixing enhancement of compressible planar mixing layer impinged by oblique shock waves. *J. Propul. Power* **31**, 156–169.